DEVELOPMENTAL NEUROSCIENCE

Osteocalcin attenuates oligodendrocyte differentiation and myelination via GPR37 signaling in the mouse brain

Zhengjiang Qian[1], Hongchao Li[1], Haiyang Yang[1,2], Qin Yang[1], Zhonghua Lu[1], Liping Wang[1], Ying Chen[3], Xiang Li[1]*

The bone-derived hormone osteocalcin (OCN) is crucial for brain development and neural cognitive functions, yet the exact roles of OCN in central nervous system (CNS) remain elusive. Here, we find that genetic deletion of *OCN* facilitates oligodendrocyte (OL) differentiation and hypermyelination in the CNS. Although dispensable for the proliferation of oligodendrocyte precursor cells (OPCs), OCN is critical for the myelination of OLs, which affects myelin production and remyelination after demyelinating injury. Genome-wide RNA sequencing analyses reveal that OCN regulates a number of G protein–coupled receptors and myelination-associated transcription factors, of which *Myrf* might be a key downstream effector in OLs. GPR37 is identified as a previously unknown receptor for OCN, thus regulating OL differentiation and CNS myelination. Overall, these findings suggest that OCN orchestrates the transition between OPCs and myelinating OLs via GPR37 signaling, and hence, the OCN/GPR37 pathway regulates myelin homeostasis in the CNS.

INTRODUCTION

Osteocalcin (OCN), encoded by both *Bglap1* and *Bglap2* genes, is solely synthesized in osteoblasts with the development of bone formation (*1*, *2*). Recently, OCN is recognized as a multifunctional bone-derived hormone that modulates numerous physiological activities and developmental processes (*3*, *4*). In peripheral organs, several studies have shown that OCN plays pivotal roles in regulating energy expenditure (*5*–*7*), male fertility (*8*, *9*), glucose homeostasis (*10*–*12*), and exercise adaptation (*13*, *14*). Besides, the ability of OCN crossing the blood-brain barrier (BBB) allows its potent regulation of neuronal functions and brain development in the central nervous system (CNS) (*15*–*18*). A specific G protein–coupled receptor (GPR), GPRC6A, has been extensively studied as the receptor for OCN in peripheral organs (e.g., adipose, liver, skeletal muscle, pancreas, and testis) and hence mediates its peripheral functions (*8*, *13*, *19*–*21*). Recent exciting reports have associated the receptor GPR158 with the transduction of OCN signal in neurons, thus mediating OCN's function in hippocampal cognition (*3*, *22*). These findings raise the possibility of OCN in exerting influences on glial cells; however, the function of OCN and its corresponding receptor in glia has not been explored yet.

Oligodendrocytes (OLs) are glial cells in the CNS that form myelin, a compact multilamellar membranous structure that wraps around axons, allows rapid saltatory conduction, and provides metabolic support to maintain axonal integrity and survival (*23*–*26*). Mature myelinating OLs are differentiated from the proliferative, migratory oligodendrocyte precursor cells (OPCs), resulting in the expression of myelinating proteins such as proteolipid protein 1 (PLP1), myelin basic protein (MBP), and 2′,3′-cyclic nucleotide phosphodiesterase (CNP) (*23*). A great number of studies have shown that CNS myelination is regulated by both inhibitory and stimulatory mechanisms including various growth factors, transcription factors, and epigenetic factors (*27*–*31*). Moreover, OL myelination is a dynamic equilibrium throughout life (*32*), while disruption of myelination leads to severe white matter diseases and the related psychiatric disorders and neurodegenerative diseases (*33*, *34*). Despite the biological significance, the underlying mechanisms of how myelin homeostasis is maintained and whether peripheral hormone is involved remain largely unknown. In the present study, we investigated the mutual cross-talk between bone-secreted OCN and glial cell functions, providing the first evidence demonstrating an essential role for OCN in the regulation of OL myelination.

Not only that, the search for OCN receptor in CNS leads us to focus on GPR37, a substrate of the E3 ubiquitin ligase parkin and originally known as parkin-associated endothelin-like receptor (*35*–*38*). GPR37 is expressed in many different brain regions and cells, particularly enriched in mature OLs (*39*, *40*), and thus plays an important role in the regulation of neuronal and glial physiology, such as dopaminergic signaling (*36*, *38*, *41*), inflammatory pain (*42*), and OL myelination (*40*). Several studies have shown that GPR37 can mediate the cellular signaling and protective effects of prosaposin and its active fragment TX14(A) on neuronal and glial cells (*42*–*44*). Here, we identified a specific ligand-receptor relationship between OCN and GPR37, proving OCN to be a bioactive molecular activating GPR37 in OL.

RESULTS

OCN deletion causes hypermyelination in the CNS

OCN can regulate neuronal functions (*3*, *16*); however, its role in OL remains unknown. To investigate whether OCN influences OL myelination, we generated OCN-deficient ($OCN^{-/-}$) mice by CRISPR-Cas9 deletion of *Bglap1* and *Bglap2* exons (fig. S1A), leading to undetectable level of OCN in cerebrospinal fluid (CSF) and serum of $OCN^{-/-}$ mice (fig. S1B). Immunostaining showed that the expression of MBP and PLP1, two major myelin proteins in CNS white matter (*25*, *45*), was markedly increased in corpus callosum (CC),

[1]Guangdong Provincial Key Laboratory of Brain Connectome and Behavior, CAS Center for Excellence in Brain Science and Intelligence Technology, Brain Cognition and Brain Disease Institute (BCBDI), Shenzhen-Hong Kong Institute of Brain Science-Shenzhen Fundamental Research Institutions, Shenzhen Institute of Advanced Technology, Chinese Academy of Sciences, Shenzhen 518055, China. [2]University of Chinese Academy of Sciences, Beijing 100049, China. [3]State Key Laboratory of Cellular Stress Biology, School of Life Sciences, Xiamen University, Xiamen 361005, Fujian, China.
*Corresponding author. Email: xiang.li@siat.ac.cn

spinal cord (SC), and cerebellum (CB) of $OCN^{-/-}$ mice in comparison to their littermate wild type (WT) at postnatal day 30 (P30) (Fig. 1, A to D, and fig. S1C). The up-regulation of myelin proteins MBP, PLP1, and MAG was validated by real-time quantitative polymerase chain reaction (qPCR) and Western blot in CC, SC, and CB of $OCN^{-/-}$ mice (Fig. 1, E to G, and fig. S1D). Next, we examined the ultrastructure of myelin sheaths in these white matter regions by electron microscopy (EM). Compared with WT, a notable increase of myelin thickness was observed in $OCN^{-/-}$ mice at P30 (Fig. 1, H and I), further confirming the hypermyelination phenotype. Moreover, the increased myelination persisted in adult $OCN^{-/-}$ mice at the age of 2 and 10 months (fig. S1E). On the basis of the analysis of EM images, we found increased severity of less tight compacted myelin sheath (fig. S1F) in $OCN^{-/-}$ mice but with unchanged myelinated axon diameter (fig. S1G) compared to WT. Together, these data indicate that ablation of OCN results in accelerated myelination in the CNS.

OCN regulates the transition of OPCs into mature OLs

The hypermyelinating phenotype of $OCN^{-/-}$ mice suggests the involvement of OCN in OPC maturation into myelinating OLs. To verify this hypothesis, the number of OPCs and mature OLs was quantified by immunostaining of their respective markers, PDGFRα (platelet-derived growth factor receptor α) and CC1. The results showed no significant change in the numbers of $PDGFR\alpha^+$ OPCs between WT and $OCN^{-/-}$ mice at P10, P20, and P30 (Fig. 2, A and B, and fig. S2, A and B). However, the quantity of $CC1^+$ mature OLs was largely increased in $OCN^{-/-}$ mice (Fig. 2, C and D, and fig. S2, C and D), indicating the precocious differentiation of OLs. To further determine the effect of OCN on OL differentiation, primary rat OPCs were isolated from neonatal cortex and induced with T3 (tri-iodothyronine) to promote cell differentiation (*31*, *46*). The process of OPC differentiation was confirmed by the expression of several key myelination genes (fig. S2E). We found that exogenous OCN treatment had no effects on OPC proliferation (Fig. 2, E and F) and OL cell viability (fig. S2F) but caused a dose-dependent reduction in the expression of myelin PLP1 and MBP (Fig. 2, G to J, and fig. S2G). Together, these observations suggest an important role of OCN in regulating the OPC differentiation into OLs.

OCN is critical for OL myelination and remyelination after demyelinating injury

Next, we further determined the role of OCN in adult myelinogenesis using $OCN^{-/-}$ and littermate WT mice. By intracerebroventricular (ICV) infusion (*16*), the synthesized mouse OCN was continuously delivered into $OCN^{-/-}$ mice for 10 days (Fig. 3A), resulting in a significant increase of the OCN level in the regions of CC and SC (fig. S3A). The supplementation of OCN rarely affected the numbers of bromodeoxyuridine-positive ($BrdU^+$)/$PDGFR\alpha^+$ proliferative OPCs (Fig. 3B) and total $PDGFR\alpha^+$ OPCs (fig. S3B) but decreased $BrdU^+/CC1^+$ differentiation OLs (fig. S3, C and D) and $CC1^+$ cells (Fig. 3C), as well as the expression of myelin PLP1 and MBP in white matter regions of $OCN^{-/-}$ mice (Fig. 3D and fig. S3, E to G). On the other hand, OCN activity was blocked by infusing OCN antibody into WT mice (Fig. 3E), leading to a significant up-regulation of PLP1 and MBP in CC region as compared with mouse immunoglobulin G (IgG) infusion (Fig. 3, F and G, and fig. S3H). Therefore, these data suggest that OCN is pivotal for the regulation of OL myelination in adult.

Given the crucial function in OL myelination, we hypothesized that OCN might also play a role in the remyelination process following lysolecithin (LPC)–induced demyelination. LPC is commonly used to induce acute myelin injury in the white matter regions (*47*, *48*). To validate this hypothesis, we stereotactically injected LPC into CC (Fig. 3H) and examined the regeneration of OLs and myelin proteins in the lesion during remyelination at 14 and 21 days post-lesion (Fig. 3I). Compared with WT, the $OCN^{-/-}$ mice show significantly enhanced myelin MBP expression (Fig. 3J) and increased $CC1^+$ OLs in the injury regions (Fig. 3, K and L). Meanwhile, the recruitment of $PDGFR\alpha^+$ OPCs to the lesion site was comparable between $OCN^{-/-}$ and WT mice (Fig. 3, M and N). Similar results showing increased remyelination and OL regeneration were also observed in SC of $OCN^{-/-}$ mice with LPC-induced lesions (fig. S3, I and J). Thus, these observations indicate that loss of OCN leads to a faster remyelination rate in LPC-induced demyelination without affecting OPC recruitment.

OCN regulates a network of genes that influence OL differentiation

To gain insight into the mechanism whereby OCN regulates OL differentiation and myelination, we carried out RNA deep sequencing and analyzed genome-wide gene expression patterns in CC from WT and $OCN^{-/-}$ mice. A total of 233 up-regulated and 355 down-regulated genes ($P < 0.05$) were identified in the $OCN^{-/-}$ mice compared with WT (Fig. 4A). The up-regulated mRNAs included a group of myelination-associated genes and transcription factors, e.g., *Plp1*, *Mbp*, *Cnp*, *Mag*, *Myrf*, and *Sox10* (Fig. 4B and fig. S4A), which are in coordination with the enhanced myelin formation phenotype in $OCN^{-/-}$ mice. Real-time qPCR validation affirmed that *Myrf* expression was negatively related to the presence of OCN in mice and primary OLs (Fig. 4C and fig. S4B). Moreover, the expression of *Myrf* was found to be dose-dependently inhibited by OCN (Fig. 4D), suggesting the involvement of *Myrf* in OCN's regulation of OL differentiation. Gene ontology (GO) analysis revealed that a group of differentially expressed genes (DEGs) was significantly enriched in gene signatures associated with lipid metabolism, transcription regulation, and myelin sheath (fig. S4C). Hence, these data suggest that OCN regulates a core network of genes that control OL differentiation.

Growing evidence suggests that the GPRs play a key role in myelinating glia (*49*), and our RNA sequencing (RNA-seq) data suggested that certain GPRs, namely, GPR17, GPR37, GPR37L1, and GPR158, may respond to OCN deletion (Fig. 4B). Among these candidates, GPR37 was verified as a significantly up-regulated receptor in $OCN^{-/-}$ mice (Fig. 4, C, E, and F, and fig. S4D). Because GPR37 has been reported as a negative regulator of OL myelination (*40*), the increase of GPR37 expression indicates a compensation function for the ablation of OCN.

OCN via GPR37 elicits intracellular responses in heterologous systems and OL

The above finding prompted us to assume that GPR37 might mediate the signal of OCN. To investigate whether OCN can activate intracellular downstream responses through binding with GPR37, we first applied several testing systems based on human embryonic kidney (HEK) 293 cells in which human GPR37 or GPR37L1, a homolog of GPR37 (*50*), was exogenously overexpressed (Fig. 5A and fig. S5, A and B). In the beginning, HEK293-GCaMP6s cells were used to measure the change of intracellular calcium level (iCa^{2+}).

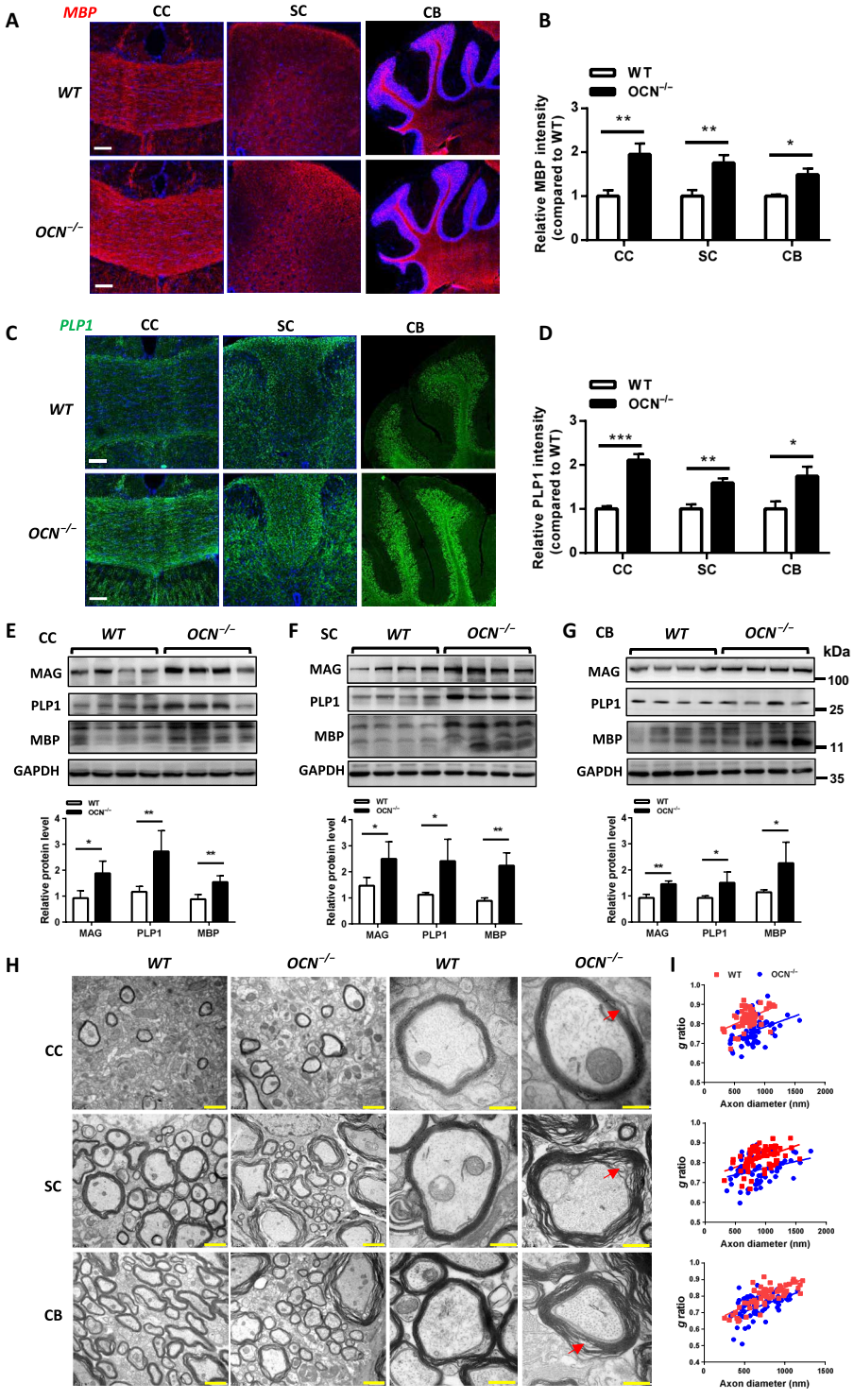

Fig. 1. *OCN*-deficient mice exhibit hypermyelination in the CNS. (**A**) Immunostaining of MBP in the CC, SC, and CB of the littermate WT and *OCN*$^{-/-}$ mice at P30. Nuclei were stained with 4′,6-diamidino-2-phenylindole (DAPI). Scale bars, 500 μm. (**B**) Relative quantification of MBP fluorescence intensity in CC, SC, and CB per area (0.25 mm^2) from (A). $n = 12$ sections from four mice per each genotype; *$P < 0.05$ and **$P < 0.01$, as compared with WT. (**C**) Immunostaining of PLP1 in CC, SC, and CB of WT and *OCN*$^{-/-}$ mice at P30. Nuclei were stained with DAPI. Scale bars, 500 μm. (**D**) Relative quantification of PLP1 fluorescence intensity in CC, SC, and CB per area (0.25 mm^2) from (C). $n = 12$ sections from four mice per each genotype; *$P < 0.05$, **$P < 0.01$, and ***$P < 0.001$, as compared with WT. (**E** to **G**) Representative immunoblot images (top panels) and relative quantification (bottom panels) of myelin-related proteins in CC (E), SC (F), and CB (G) of WT and *OCN*$^{-/-}$ mice at P30. $n = 4$ mice; *$P < 0.05$ and **$P < 0.01$, as compared with WT. (**H** and **I**) Representative electron micrographs (H) and *g* ratio as a function of axonal diameter analysis (I) of CC, SC, and CB in WT and *OCN*$^{-/-}$ mice at P30. Red arrows indicate a less compactness of myelin sheath in *OCN*$^{-/-}$ mice. Scale bars, 2 μm [left two panels in (H)] and 0.2 μm [right two panels in (H)]. $n = 12$ sections from four mice per each genotype.

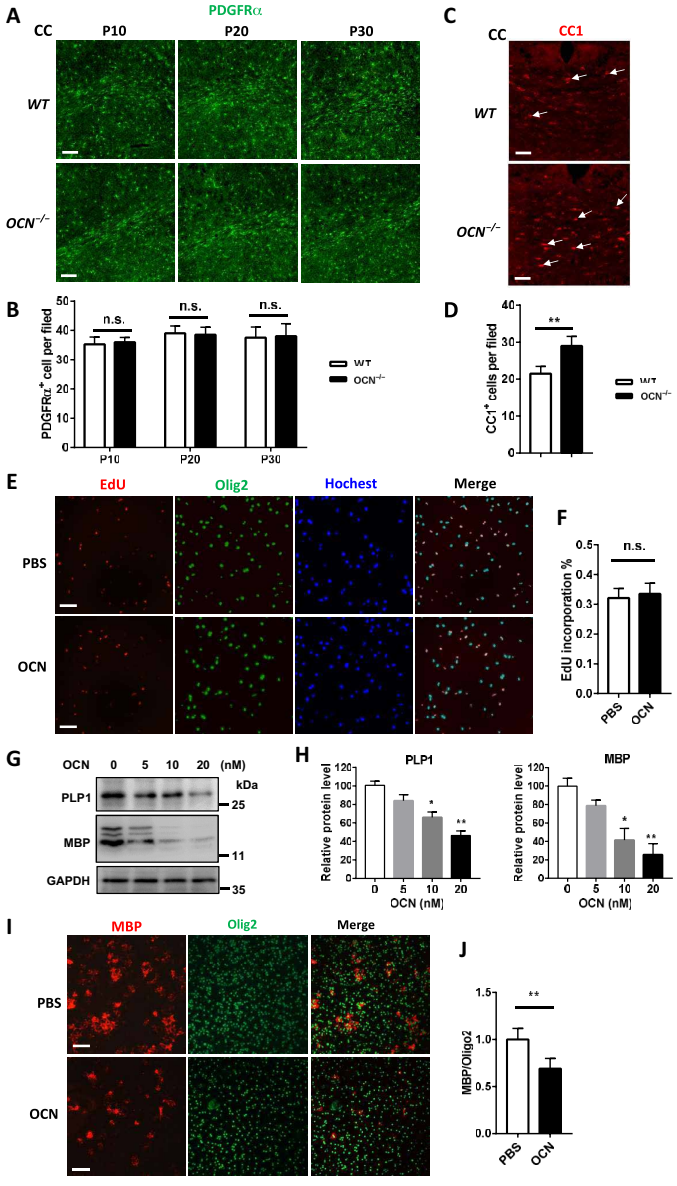

Fig. 2. OCN regulates the transition of OPCs into differentiated OLs. (**A**) Immunostaining of PDGFRα in the CC of WT and *OCN*$^{-/-}$ mice at P10, P20, and P30. Scale bars, 500 μm. $n = 12$ sections from three mice per each genotype. (**B**) Quantification of PDGFRα^{+} OPCs per area (0.25 mm^2) in CC from WT and *OCN*$^{-/-}$ mice from (A). $n = 3$ mice for each group; n.s., nonsignificant change. (**C**) Immunostaining of CC1 in CC of WT and *OCN*$^{-/-}$ mice at P30. Arrows indicate the labeled cells. Scale bars, 500 μm. $n = 12$ sections from three mice per each genotype. (**D**) Quantification of CC1^{+} mature OLs per area (0.25 mm^2) in CC from WT and *OCN*$^{-/-}$ mice at P30. $n = 3$ mice for each group; $^{**}P < 0.01$, as compared with WT. (**E**) Effect of OCN (20 nM) treatment on proliferation of primary rat OPCs by EdU labeling assay. Scale bars, 50 μm. $n = 3$ independent experiments. (**F**) Quantification of EdU incorporation rate in (E). (**G** and **H**) Effect of OCN concentration on the expression of myelin-related proteins in primary rat OPCs cultured in differentiation medium. Representative immunoblot images (G) and relative quantification (H) were shown. $n = 3$ independent experiments; $^{*}P < 0.05$ and $^{**}P < 0.01$, as compared with PBS. (**I** and **J**) Immunostaining of MBP (I) and relative quantification of MBP fluorescence intensity (J) in primary rat OPCs in differentiation medium in the presence of OCN (20 nM). Scale bars, 50 μm. $n = 3$ independent experiments; $^{**}P < 0.01$, as compared with PBS.

We found that OCN elicited a rapid and robust increase of iCa^{2+} in GPR37, but not GPR37L1, overexpressed cells (Fig. 5B). Yet, the increase of iCa^{2+} was abolished by the pretreatment of GPR37 antibody or pertussis toxin (PTX) (fig. S5C), an inhibitor of the $G\alpha_{i/o}$-coupled pathway (*43*). As additional positive controls, the effectiveness of OCN and HEK293-GCaMP6s testing system was confirmed by expressing GPRC6A and GPR158 (fig. S5D), two reported receptors of OCN (*19*, *22*, *51*), and the application of prosaptide TX14(A) (fig. S5E), a known ligand for both GPR37 and GPR37L1 (*43*). Second, a PRESTO-Tango GPCR assay system (*52*) was used to determine whether OCN could activate β-arrestin recruitment through GPR37 in HTLA cells (Fig. 5C). We found that both OCN and TX14(A) induced a dose-dependent increase of luciferase activity in GPR37-transfected cells with an EC_{50} (median effective concentration) of 10.2 ± 2.5 nM and 19.4 ± 1.8 nM (Fig. 5C and fig. S5F). In contrast to TX14(A), OCN failed to exert luciferase responses in cells expressing GPR37L1 (Fig. 5C and fig. S5F). Third, consistent with previous studies that the activation of GPR37 was coupled to intracellular adenosine 3′,5′-monophosphate (cAMP) and extracellular signal–regulated kinase (ERK) signals (*40*, *43*), we found that OCN significantly inhibited cAMP production and stimulated ERK phosphorylation in GPR37-transfected, but not GPR37L1-transfected, cells (Fig. 5, C, E, and F). These effects of OCN were markedly blocked by pretreatment of GPR37 antibody or PTX (fig. S5G). Last, binding affinity assay revealed that biotinylated OCN bound to GPR37 rather than GPR37L1 with a dissociation constant (K_d) of 14.1 ± 1.8 nM (Fig. 5F). The direct interaction of OCN with GPR37 was further supported by coimmunoprecipitation assay (Fig. 5G). Together, these results reveal that OCN specifically interacts with GPR37 to trigger various intracellular downstream signaling in heterologous expression systems.

Because GPR37 is highly expressed in mature OLs (*37*, *40*), we then went on to test whether OCN also takes action in primary rat OLs. The GPR37 level is barely detected in OPCs but rapidly increased after T3-induced differentiation into OLs (fig. S5, H and I). Thus, we silenced GPR37 expression in mature OLs by using short hairpin RNA (shRNA) (fig. S5, J and K) and found that OCN-induced inhibition of intracellular cAMP production was substantially prevented (Fig. 5H). Similar to the HEK293 cell studies, PTX pretreatment also blocked OCN-caused reduction of the intracellular cAMP level and boost of ERK phosphorylation in myelinating OLs (Fig. 5, H and I). Therefore, these data indicated that OCN also elicits intracellular signals through GPR37 in primary OLs. Consistent with a previous study of *GPR37*$^{-/-}$ mice (*40*), we also found that the cAMP and pERK levels were increased in the brain of *OCN*$^{-/-}$ mice (fig. S5, L and M).

GPR37 is required for OCN's regulation of OL differentiation and myelination

To determine the role of GPR37 in mediating OCN's function in primary OLs, the activity of GPR37 was blocked by either shRNA or antibody. As a consequence, OCN-induced inhibition of PLP1 and MBP expression was significantly suppressed in primary OLs (Fig. 6, A to D, and fig. S6A). The specificity of this OCN/GPR37 effect was further supported by silencing of GPR37L1, which was unable to inhibit OCN's suppression of the MBP level (fig. S6, B and C). Furthermore, we isolated primary OPC from *GPR37*$^{-/-}$ mice and then induced it with T3. It was shown that myelin MBP was unresponsive to OCN treatment unless the GPR37 level was restored,

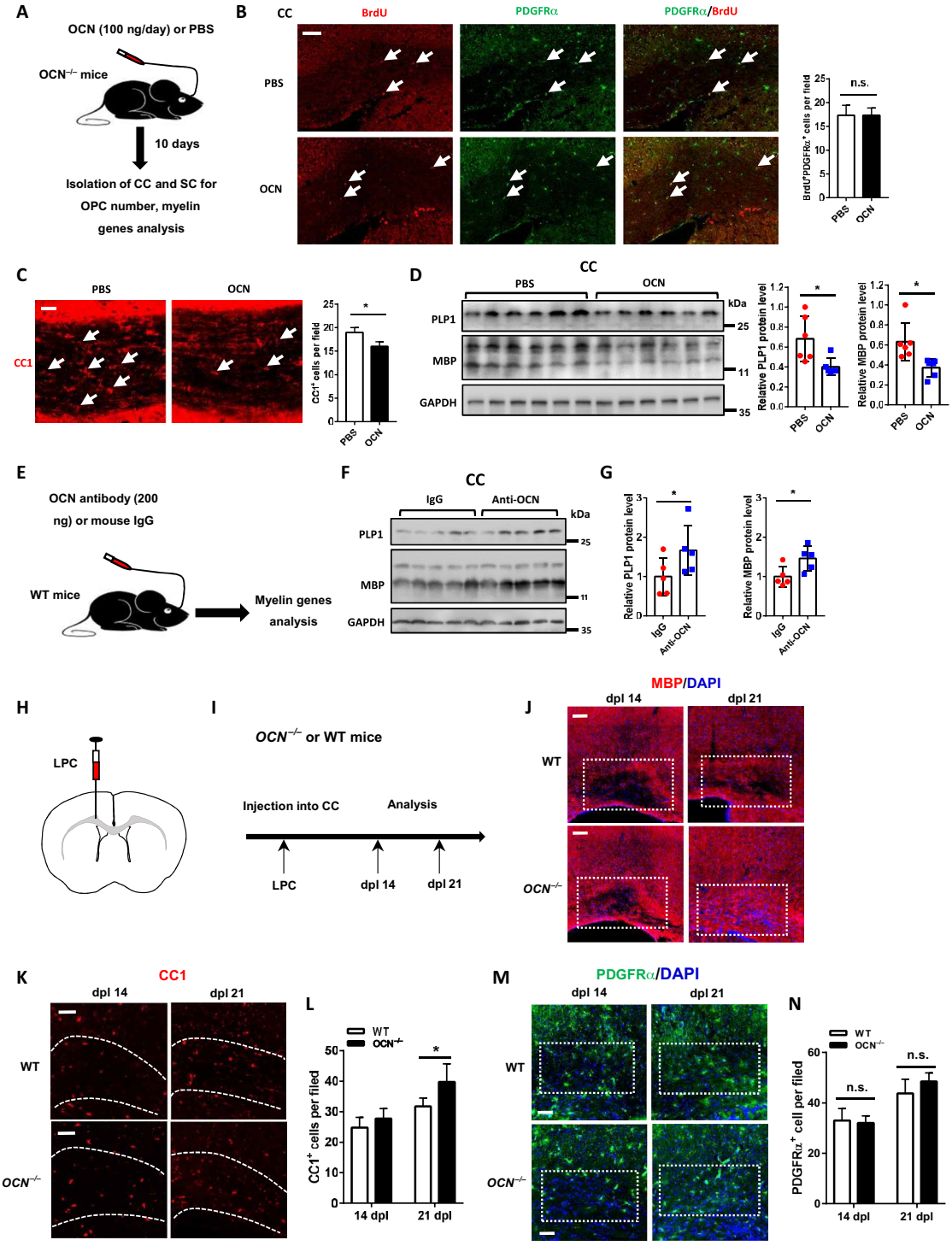

Fig. 3. OCN is critical for OL myelination and remyelination after demyelination. (**A**) Diagram showing experiments of OCN delivery into *OCN*$^{-/-}$ mice via ICV. (**B** and **C**) Immunostaining and quantification of BrdU^{+}/ PDGFRα^{+} OPCs (B) and CC1^{+} mature OLs (C) per area (0.25 mm^{2}) in CC of *OCN*$^{-/-}$ mice infused with PBS or OCN. Scale bars, 500 μm. $n = 12$ sections each group. *$P < 0.05$ compared with PBS. (**D**) Representative immunoblot images and relative quantification showing the effects of OCN delivery on the expression of myelin proteins in CC of *OCN*$^{-/-}$ mice infused with PBS or OCN. $n = 6$ mice; *$P < 0.05$, compared with PBS. (**E**) Diagram showing experiments of OCN antibody delivery into WT mice. (**F** and **G**) Representative immunoblot images (F) and relative quantification (G) showing the effects of OCN antibody delivery on the expression of myelin proteins in CC of WT mice. $n = 5$ mice. *$P < 0.05$, compared with IgG. (**H** and **I**) Diagram showing LPC injection site (H) and experimental schedule (I). (**J**) Immunostaining of MBP in CC lesions of WT and *OCN*$^{-/-}$ mice at 14 and 21 days post-lesion (dpl 14 and dpl 21). Scale bars, 500 μm. $n = 3$ mice. (**K** and **L**) Immunostaining of CC1 (K) and quantification of CC1^{+} mature OLs per area (0.25 mm^{2}) (L) in LPC-induced lesions at dpl 14 and dpl 21. Scale bars, 200 μm. $n = 3$ mice; *$P < 0.05$, compared with WT. (**M** and **N**) Immunostaining of PDGFRα^{+} (M) and quantification of PDGFRα^{+} cells per area (0.25 mm^{2}) (N) in LPC-induced lesions at dpl 14 and dpl 21. Scale bars, 200 μm. $n = 3$ mice.

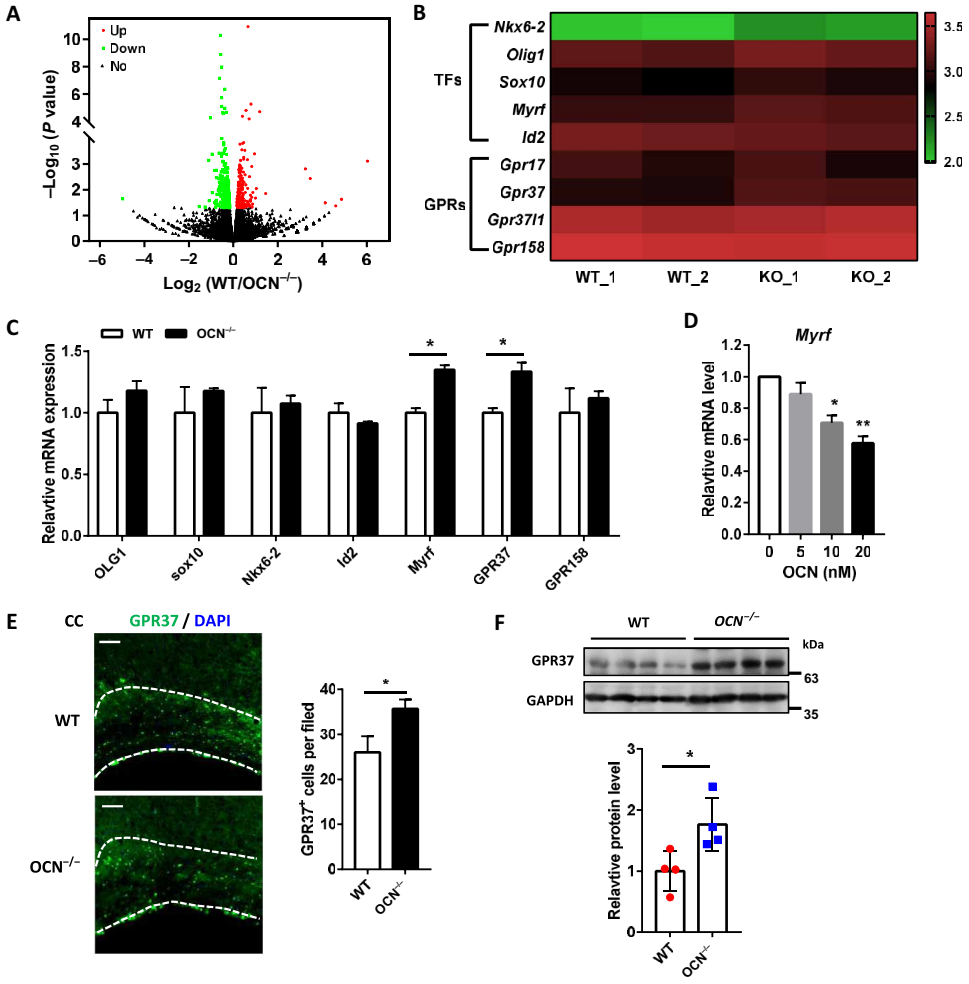

Fig. 4. OCN regulates a group of genes that influence OL differentiation. (**A**) Volcano plot of genes differentially expressed in CC from WT and *OCN*$^{-/-}$ mice. The up-regulated, down-regulated, and no significant changed genes were indicated as red, green, and black blots, respectively. $n = 2$ mice for each group; $P < 0.05$. (**B**) Heatmap of differentially expressed myelin-associated transcription factors (TFs) and GPRs from RNA-seq. (**C**) Real-time qPCR analyses validated the expression of myelin-associated transcription factors and GPRs in WT and *OCN*$^{-/-}$ mice. $n = 6$ mice; $^{*}P < 0.05$, as compared with WT. (**D**) The expression of *Myrf* was dose-dependently inhibited by OCN stimulation in primary rat OLs. $n = 3$ independent experiments; $^{*}P < 0.05$ and $^{**}P < 0.01$, as compared with PBS. (**E**) Immunostaining of GPR37 (left) and relative quantification of fluorescence intensity (right panel) in the CC of WT and *OCN*$^{-/-}$ mice. Scale bars, 500 μm. $^{*}P < 0.05$, as compared with WT. (**F**) Representative immunoblot images (top) and relative quantification (bottom) of GPR37 in CC of WT and *OCN*$^{-/-}$ mice. $n = 4$ mice; $^{*}P < 0.05$, as compared with WT.

which then resulted in down-regulation of MBP expression (fig. S6D). Similar to myelin protein, the down-regulation of *Myrf* by OCN treatment was also abolished by knockdown of GPR37 in primary OLs (fig. S6E), suggesting an important role for *Myrf* in the downstream of OCN/GPR37 signaling.

To further confirm the above finding, we carried out in vivo studies using *GPR37*$^{-/-}$ and littermate WT mice. In situ hybridization and Western blotting analysis exhibited that GPR37 was highly enriched in SC and CC of WT mice but was undetectable in those regions of *GPR37*$^{-/-}$ mice (fig. S6F). By ICV infusion, we found that exogenous OCN delivery induced a significant down-regulation of myelin PLP1 and MBP in CC of WT mice (Fig. 6, E and F), while these effects of OCN were absent in *GPR37*$^{-/-}$ mice (Fig. 6, G and H). Similar results were also observed in SC of WT and *GPR37*$^{-/-}$ mice in response to OCN delivery (fig. S6, G and H). Accordingly, the injection of lentivirus overexpressing GPR37 led to a significant reduction of PLP1 and MBP expression in CC of *GPR37*$^{-/-}$ mice (Fig. 6, I and J). Collectively, these data suggested that GPR37 is required for OCN's regulation of OL differentiation and myelination.

GPR37 negatively regulates CNS myelination

We next determined the role of GPR37 in CNS myelination. Compared with the littermate WT, a significant elevated thickness of myelin sheath was observed in SC and CC of *GPR37*$^{-/-}$ mice by EM (fig. S7, A and B). To have a straightforward visualization, 1-cm length of SC tissue was analyzed at a larger scale (micrometer level) using an x-ray microscope (ZEISS Xradia 510 Versa, Carl Zeiss). By scanning the SC from different dimensional sections and the subsequent reconstruction to three-dimensional (3D) conformation, a remarkable increase of white matter thickness was observed in *GPR37*$^{-/-}$ compared to WT mice (Fig. 7, A and B, and fig. S7, C to E).

To further verify the function of GPR37, we selectively ablated GPR37 in OL lineage cells by breeding GPR37$^{loxP/loxP}$ mice with an OL lineage expressing Olig2-Cre line that commences during OPC

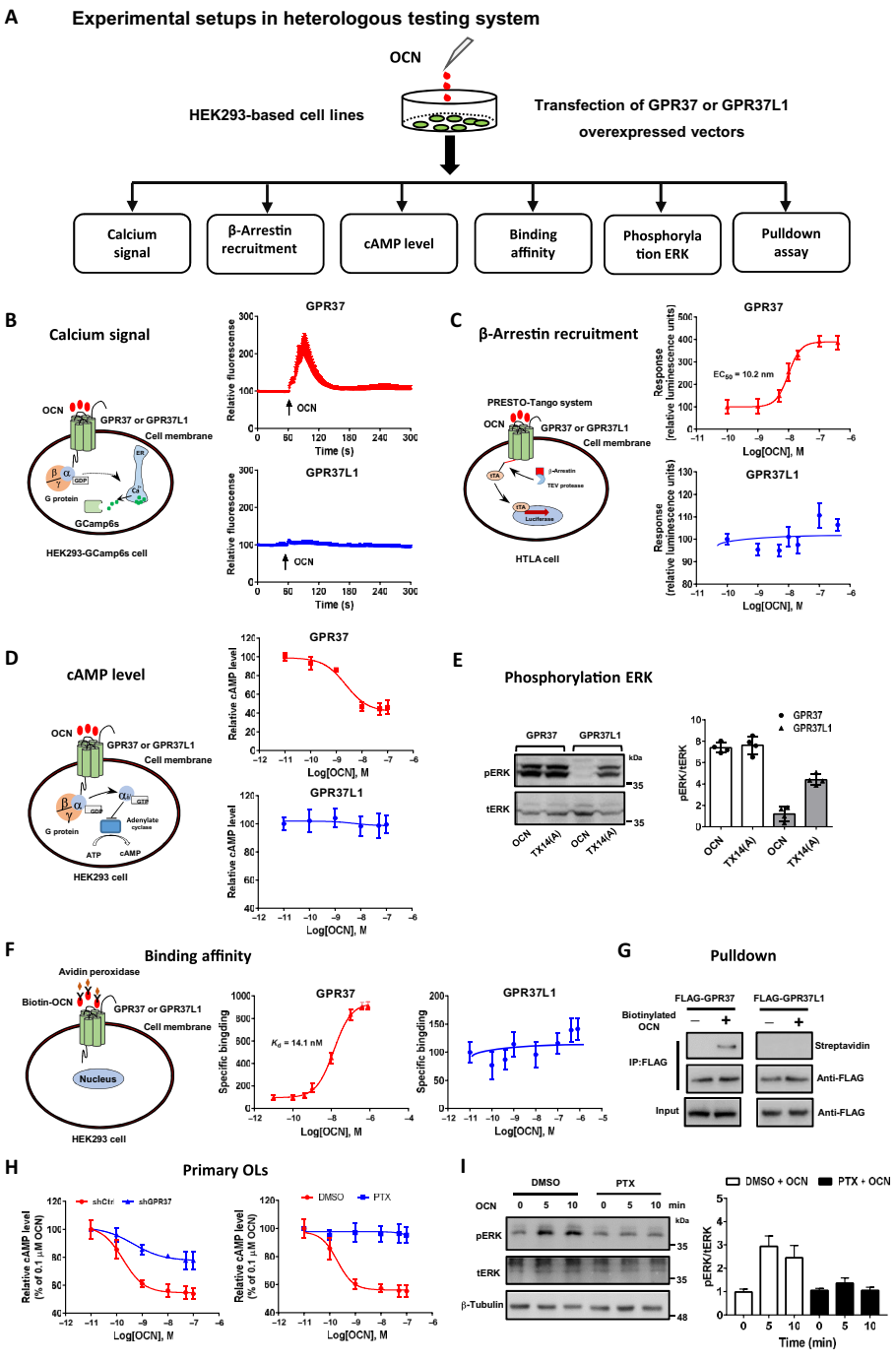

Fig. 5. GPR37 mediates OCN-induced intracellular responses in HEK293 cells and primary OLs. (**A**) Overview of the experimental design in HEK293-based heterologous testing systems. Human GPR37 or GPR37L1 was exogenously overexpressed in HEK293-based cell lines for the study of intracellular calcium level (iCa^{2+}), β-arrestin recruitment, cAMP production, pERK level, binding affinity, and pulldown assay in response to OCN treatment. (**B**) Schematic diagram of iCa^{2+} detection (left one) and representative response curve of OCN-triggered iCa^{2+} changes (right two) in GPR37- or GPR37L1-transfected HEK293-GCaMP6s (a HEK293 cell line stably expressing GCaMP6s) cells. (**C**) Schematic diagram of β-arrestin recruitment assay (left one) and representative concentration-response curve of OCN-triggered luciferase activity (right two) in GPR37- or GPR37L1-transfected HTLA (a HEK293 cell line stably expressing a tTA-dependent luciferase reporter and a β-arrestin2–TEV fusion protein) cells by a PRESTO-Tango system. (**D**) Schematic diagram of cAMP production (left one) and concentration-response curve of OCN-triggered inhibition of cAMP production (right two) in GPR37- or GPR37L1-transfected HEK293 cells. (**E**) The pERK level was induced by OCN (20 nM) treatment in GPR37-transfected, but not GPR37L1-transfected, HEK293 cells. (**F**) Schematic diagram of binding affinity assay (left one) and saturation curves of OCN binding (right two) in GPR37- or GPR37L1-transfected HEK293 cells. (**G**) Pulldown assay showing that OCN directly interacts with GPR37 in HEK293 cells. (**H**) Concentration-response curve of OCN-triggered inhibition of cAMP production in primary rat OL cells with GPR37 knockdown (left) or PTX pretreatment (right). (**I**) Representative immunoblot images (left) and relative quantification (right) showing that PTX pretreatment blocked OCN-triggered increase of the pERK level in primary rat OLs.

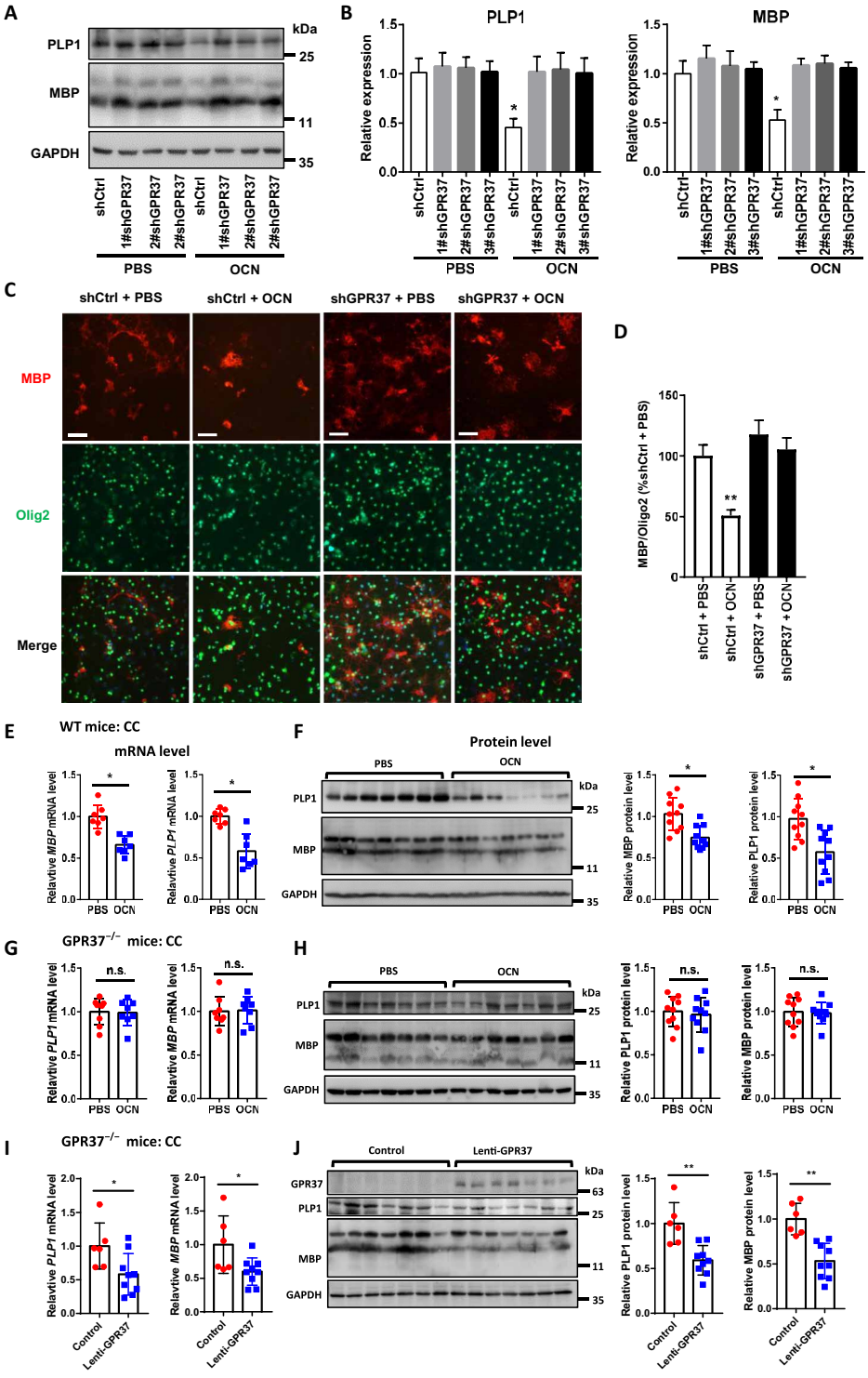

Fig. 6. GPR37 is required for OCN's regulation of OL myelination. (**A** and **B**) Representative immunoblot image (A) and relative quantification (B) showing the effect of GPR37 knockdown on the expression of PLP1 and MBP protein in primary rat OLs in the presence of OCN (20 nM). $n = 3$ independent experiments; $^{*}P < 0.05$, as compared with PBS. (**C** and **D**) Representative staining images (C) and relative quantification (D) showing the immunostaining of MBP in primary rat OLs in the presence of OCN (20 nM). Scale bars, 50 μm. $n = 3$ independent experiments; $^{**}P < 0.01$, as compared with PBS. (**E** and **F**) Effects of OCN delivery on the expression of myelin PLP1 and MBP in CC of WT mice at the mRNA level (E) and the protein level (F). $n \geq 6$ mice; $^{*}P < 0.05$, as compared with PBS infusion. (**G** and **H**) Effects of OCN delivery on the expression of myelin PLP1 and MBP in CC of *GPR37*$^{-/-}$ mice at the mRNA level (G) and the protein level (H). $n \geq 6$ mice. (**I** and **J**) Effects of GPR37 restoration on the expression of myelin PLP1 and MBP in CC of *GPR37*$^{-/-}$ mice at the mRNA level (I) and the protein level (J). $n = 6$ mice; $^{*}P < 0.05$ and $^{**}P < 0.01$, as compared with control.

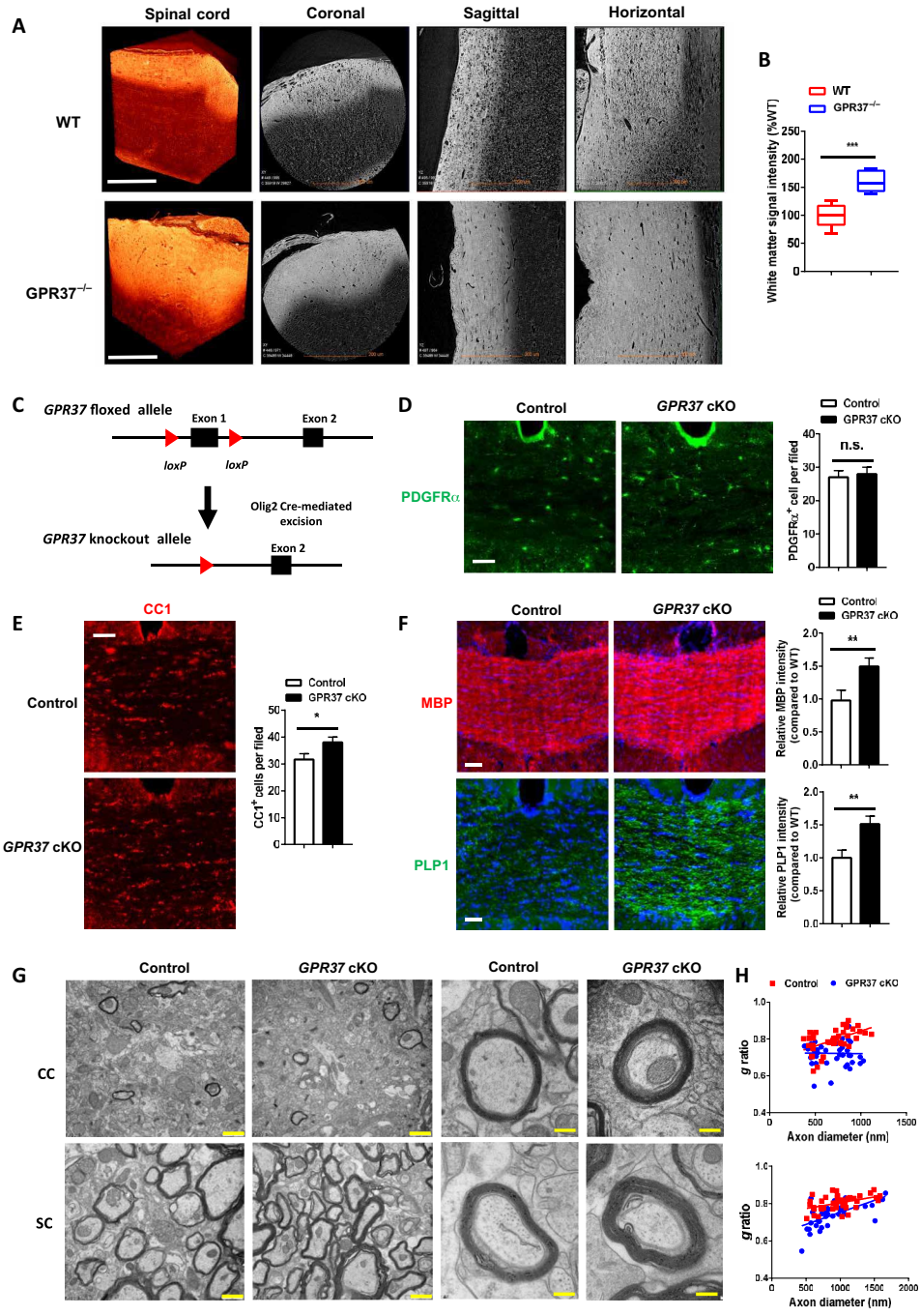

Fig. 7. GPR37 negatively regulates OL myelination in CNS. (**A** and **B**) X-ray microscope analysis of SC in WT and *GPR37*$^{-/-}$ mice. Representative images of coronal, sagittal, and horizontal sectional views (A) and relative quantification of white matter signal intensity (B) were shown. Scale bars, 200 μm. $n = 3$ mice; ***$P < 0.001$, as compared with WT. (**C**) Schematic diagram depicting the strategy used to generate GPR37 LoxP/LoxP mice and Cre-mediated excision of the floxed GPR37. (**D**) Immunostaining PDGFRα (left) and quantification of PDGFRα$^+$ OPCs per area (0.25 mm^2) (right) in CC of the GPR37 cKO mice. Scale bar, 500 μm. $n = 3$ mice. (**E**) Immunostaining CC1 (left) and quantification of CC1$^+$ mature OLs per area (0.25 mm^2) (right) in CC of the GPR37 cKO mice. Scale bar, 500 μm. $n = 3$ mice; *$P < 0.05$, as compared with control. (**F**) Immunostaining of MBP, PLP1, and their relative quantification of intensity in CC of the GPR37 cKO mice. Scale bars, 500 μm. $n = 3$ mice; **$P < 0.01$, as compared with control. (**G** and **H**) Electron micrographs (G) and *g* ratio as a function of axonal diameter analysis (H) of CC and SC in control and GPR37 cKO mice at P30. Scale bars, 2 μm (left two panels) and 0.2 μm (right two panels). $n = 12$ sections from four mice per each genotype.

development (Fig. 7C). The conditional GPR37 knockout mice (GPR37$^{fl/fl}$; Olig2-Cre, hereafter referred to as GPR37 cKO mice) were compared with their littermate controls (GPR37$^{fl/fl}$; Olig2-Cre or GPR37$^{fl/fl}$ mice, phenotypically normal in OL development). A similar number of PDGFRα$^+$ OPCs were found between control and GPR37 cKO mice (Fig. 7D), while increased CC1$^+$ mature OLs (Fig. 7E), up-regulated myelin MBP and PLP1 expression (Fig. 7F), and elevated thickness of myelin sheath were observed in GPR37

cKO mice (Fig. 7, G and H). Together, these data suggest a specific function of GPR37 in the regulation of CNS myelination.

Deletion of OCN and GPR37 results in delayed conduction

Because it has been well recognized that myelination is crucial for saltatory conduction of impulses (*53*), we then asked whether the dysregulation of CNS myelination in *OCN*$^{-/-}$ and *GPR37*$^{-/-}$ mice can cause abnormal conduction. First, we carried out hot plate test (Fig. 8A), which is related to pain sense reflex that involved both cerebral and spinal mediated circuits (*54*). As compared with the controls, a significant increase of paw lick latency was observed in *OCN*$^{-/-}$, *GPR37*$^{-/-}$, and GPR37 cKO mice responding to heat stimulation (Fig. 8B), indicating a delayed conduction in sense of pain. To determine whether OCN is sufficient for the resolution of pain sense, we performed an intraperitoneal injection of OCN (Fig. 8C). Strikingly, the deficit of thermal sensitivity in the *OCN*$^{-/-}$ mice was partially rescued by infusion of OCN (Fig. 8D). Moreover, the change of conduction was also evaluated by pupillary light reflex (Fig. 8E), a commonly used clinical method to observe the amount of pupil contraction in response to light as it is alternated between the two eyes (*55*). Consistent with hot plate test, both *OCN*$^{-/-}$ and *GPR37*$^{-/-}$ mice showed delayed response to light stimulation by taking longer afferent input time and pupillary convergence (Fig. 8F), while supplementation of OCN partially recovered these retarded responses in *OCN*$^{-/-}$ mice (Fig. 8, G and H). By contrast, grip strength analysis and open-field test revealed that the forelimb grip strength and locomotor activity of *OCN*$^{-/-}$ and *GPR37*$^{-/-}$ mice are similar to their respective controls (fig. S8).

DISCUSSION

Despite that promising progress has been achieved, deciphering the diverse functions of OCN and the underlying molecular mechanisms in CNS is still far to be illuminated (*3*, *16*, *22*, *51*). In the present study, we demonstrate that OCN, via interaction with the specific receptor GPR37, plays a critical role in the regulation of OL differentiation and myelination through the downstream transcription factor Myrf in the CNS (Fig. 8I). Our work also suggested that the regulatory axis of OCN and GPR37 could be a vital mechanism to maintain myelin homeostasis during development, thereby providing a unique perspective for the understanding of mutual communication between the skeleton biology and glial functions.

OCN plays a functional role in CNS glial cells

Accumulative work indicate that OCN can cross the BBB and bind specifically with neurons in different brain regions such as dorsal raphe nuclei (DRN) and medial raphe nuclei (MRN) of the brainstem, the ventral tegmental area (VTA) of the midbrain, and the cornu ammonis 3 (CA3) region of the hippocampus (*3*). Upon binding, OCN can trigger signals in these neurons to promote the synthesis of monoamine neurotransmitters (e.g., serotonin, dopamine, and noradrenaline) and reduce the synthesis of γ-aminobutyric acid (GABA), and these cellular and molecular activities may contribute to the improvement in spatial learning and memory and anxiety-like behaviors (*16*, *22*, *51*). However, it remains unknown whether OCN has a potential role in regulating glial functions in CNS. In this work, we showed that ablation of OCN causes increased expression of myelin-related genes, accelerated CNS myelination, and enhanced thickness of myelin sheath but has no influences on cell proliferation and viability. In addition, OCN deletion also facilitated remyelination after LPC-induced demyelination. Consistent with these scenarios, blocking OCN activity by antibody neutralization resulted in up-regulation of myelin proteins in WT mice, while exogenous supplementation of OCN decreased the expression of myelin genes in both in vitro (primary OLs) and in vivo (WT and *OCN*$^{-/-}$ mice) studies. Therefore, these findings demonstrate that OCN is essential for the development of glial OLs, expanding the field of OCN's function in the CNS. A less compacted myelin sheath was prone to be found in *OCN*$^{-/-}$ mice, which could be related to the dysregulated expression of myelin gene and lipid metabolism in OLs, yet further in-depth work needs to be performed.

GPR37 acts as a novel receptor for OCN

Another important discovery of this study is that we identified GPR37 as a specific receptor for OCN in OLs. First, several signaling testing methods were applied to provide a range of robust evidences that OCN, by directly interacting with GPR37, elicits a series of intracellular responses in both heterologous expressing systems and primary OL cells. By contrast, GPR37L1, a homolog of GPR37, was unable to mediate these effects of OCN. It should be noted that the pERK level was triggered by OCN stimulation in GPR37-transfected HEK293 and OLs, which seems to conflict with the increase of pERK in *OCN*$^{-/-}$ and *GPR37*$^{-/-}$ mice (*40*). The discrepancy could be due to the difference in experimental conditions, i.e., the former one was performed in cells with short-term treatment (no more than 10 min), thus indicating a transient effect of OCN in GPR37 signaling, while the latter one was conducted in animals that showed a long-term GPR37 function under the $G_{i/o}$ protein–coupled pathway. Moreover, we further showed that suppression of GPR37 activity, by either shRNA interference or antibody blocking, abolished the OCN-induced down-regulation of myelination proteins in OLs. Accordingly, restoration of GPR37 reclaimed the effects of OCN on primary OLs derived from *GPR37*$^{-/-}$ mice. Thus, these in vitro experiments indicate that GPR37 is required for OCN's signaling and regulation of OL differentiation. On the other hand, our in vivo study demonstrated that the *GPR37*$^{-/-}$, but not WT, mice resisted to the inhibitive effects of OCN delivery on myelin protein expression, whereas recovery of the GPR37 level rescued OCN's regulation of OL myelination and CNS hypermyelination in *GPR37*$^{-/-}$ mice. In addition, we further showed that specific depletion of GPR37 in OL lineage led to accelerated myelination. Together, we conclude that GPR37 acts as a receptor for OCN and mediates its function in OLs. Moreover, because GPR37 is not present in myelinating Schwann cell (*40*, *56*), the action of the OCN/GPR37 regulatory axis on myelination could be specific in OL.

Myrf might be a key regulator mediating the signal of the OCN/GPR37 axis

The growth and maturation of OL lineage is controlled by a complex regulatory transcriptional network (*40*, *57*, *58*). In this study, we identified *Myrf*, a key transcription factor for OL myelination and myelin maintenance (*58*, *59*), as a significantly up-regulated gene in the absence of OCN. Although alteration in the number of mature OLs could contribute to the expression of *Myrf* in *OCN*$^{-/-}$ mice, the in vitro study using T3-induced primary OLs revealed that the *Myrf* level could be dose-dependently inhibited by OCN treatment. OCN-caused down-regulation of *Myrf* was abolished by shRNA interference of GPR37, which is coordinated with the observation

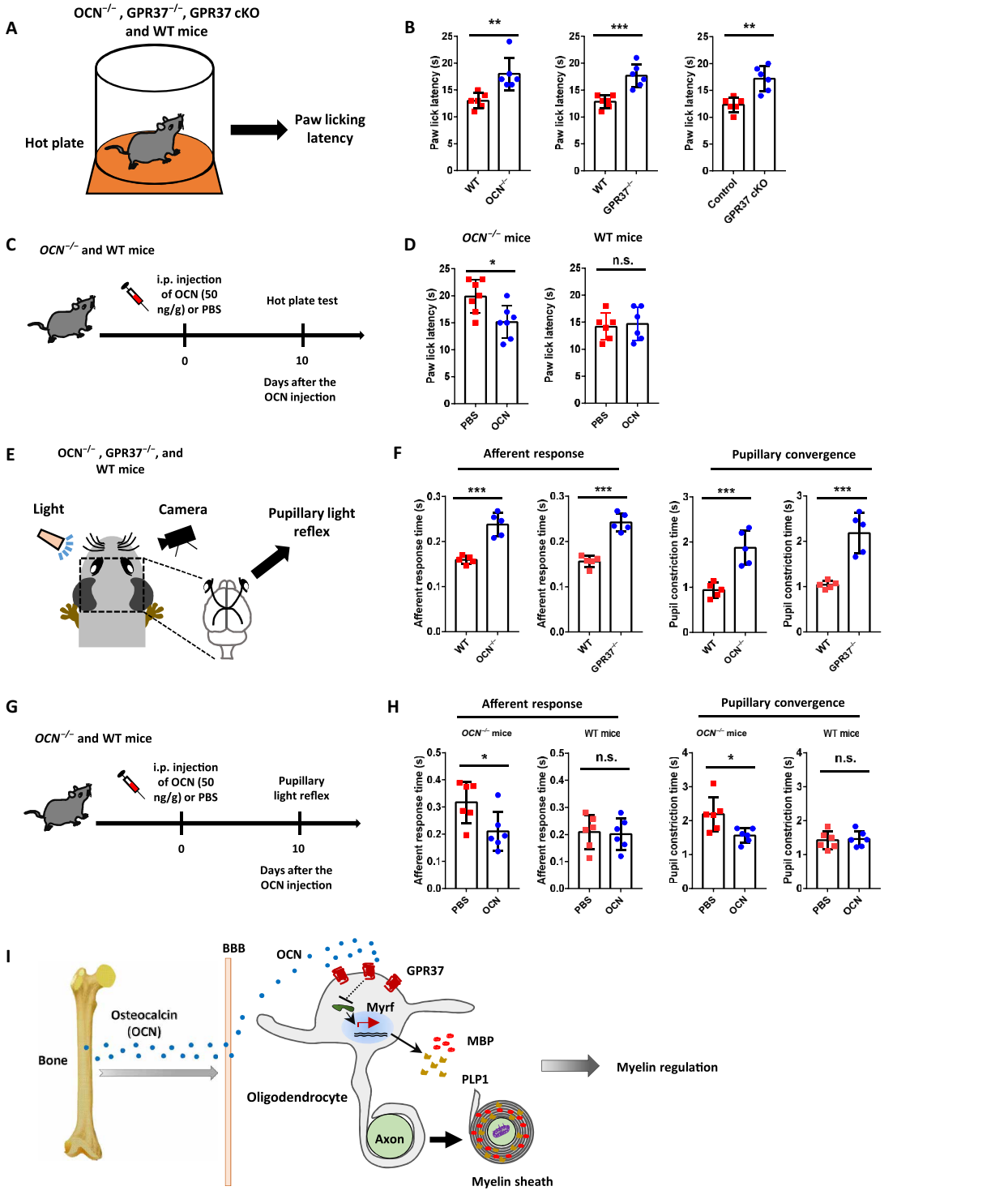

Fig. 8. *OCN*$^{-/-}$ and *GPR37*$^{-/-}$ mice show delayed conduction. (**A**) Schematic diagram showing hot plate test. (**B**) Quantification of paw lick latency in *OCN*$^{-/-}$, *GPR37*$^{-/-}$, and GPR37 cKO mice in response to heat stimulation. $n = 6$ mice; $^{**}P < 0.01$ and $^{***}P < 0.001$, as compared with WT. (**C**) Experimental diagram showing the timeline of intraperitoneal (i.p.) injection of OCN and hot plate test. (**D**) Quantification of paw lick latency after intraperitoneal injection of OCN in *OCN*$^{-/-}$ and WT mice. $n \geq 6$ mice; $^{*}P < 0.05$, as compared with PBS. (**E**) Schematic diagram showing the pupillary light reflex experiment. (**F**) Quantification of afferent response time and pupil constriction time in *OCN*$^{-/-}$ and *GPR37*$^{-/-}$ in response to light. $n = 5$ mice; $^{***}P < 0.001$, as compared with WT. (**G**) Experimental diagram showing the timeline of intraperitoneal injection of OCN and pupillary light reflex experiment. (**H**) Quantification of afferent response time and pupil constriction time after intraperitoneal injection of OCN in *OCN*$^{-/-}$ and WT mice. $n = 5$ mice; $^{*}P < 0.05$, as compared with PBS. (**I**) Schematic mechanism depicting the action of OCN on myelin regulation in OL, whereby the receptor GPR37 mediates the effects of OCN by inhibiting *Myrf* (myelin gene regulatory factor) to down-regulate the expression of myelin genes.

that the down-regulation of myelin PLP1 and MBP by OCN could be prevented by blocking GPR37 activity both in vivo and in vitro. Moreover, a previous study has shown that the expression of *Myrf* is increased in *GPR37*$^{-/-}$ mice (*40*). Because *Myrf* is known to maintain CNS myelination by modulating the expression of myelin genes (*58*, *59*), our results suggested that *Myrf* might be a key effector that at least partially mediated the downstream function of OCN and GPR37 signaling in myelination OLs. Nevertheless, the exact regulatory mechanism of how Myrf is regulated and the related molecular mechanisms should be further investigated.

The OCN/GPR37 axis may implicate in saltatory conduction

Previous works have shown that OCN can regulate anxiety and cognitive functions (*3*, *16*, *22*), and the Parkinson's disease–associated GPR37 is involved in the regulation of locomotor behavior (*38*, *60*). The authors attributed these physiological roles of OCN and GPR37 to their influence on neuronal functions. From the view of glial cell, there is growing evidence that proper OL myelination is critical in facilitating and shaping behavior and brain functions, while disturbance of myelin homeostasis disrupts saltatory nerve conduction, neuronal cognitive, or motor functions, thus contributing to neuropsychiatric diseases (*26*, *53*, *61*). In this work, we demonstrated that both *OCN*$^{-/-}$ and *GPR37*$^{-/-}$ mice developed aberrant OL myelination, which would potentially affect the function of neuron and partially contribute to their deficient behaviors. In support of this notion, we found a remarkable delayed conduction of pain sense reflex and pupillary light reflex in these two mouse lines, while infusion of OCN partially recovered the defective responses in *OCN*$^{-/-}$ mice. However, no significant changes in forelimb grip strength and locomotor activity were observed. Hence, these finding implied a distinguishing role of the OCN/GPR37 axis in mediating impulse transmission. A variety of parameters affecting action potential conduction have been proposed in the CNS, including axonal diameter, myelin thickness, number of Ranvier nodes, the length of the nodal gap, and the clustering of sodium channels in Ranvier node (*62*, *63*). Notably, our results showed a prolonged conduction despite increased myelin thickness in *OCN*$^{-/-}$ and *GPR37*$^{-/-}$ mice. Because there are no significant changes in axonal diameter of myelinated axon, the possible reason could be the inappropriate compactness of myelin sheath, which might, in turn, cause abnormal change of sodium channel nodal clustering or internodal length. Nevertheless, the exact regulatory mechanism remains to be elucidated in depth.

In summary, we demonstrate that OCN and GPR37 form a vital regulatory mechanism in modulation of OL differentiation and myelination, and their mutual interactions could contribute to the maintenance of myelin homeostasis in CNS. Hence, our findings may have potential therapeutic implications for demyelinating and other neurological diseases involving white matter pathology.

MATERIALS AND METHODS

Mice and treatment

All mice were bred in specific pathogen–free facilities at Shenzhen Institute of Advanced Technology (SIAT), Chinese Academy of Sciences. All experimental procedures were performed according to protocols approved by the Institutional Animal Care and Use Committee at SIAT. Mice were housed in a vivarium with 12-hour light/12-hour dark cycle with free access to water and food. The *OCN*$^{-/-}$ and GPR37$^{loxP/loxP}$ mice were generated using CRISPR-Cas9 technique by model organisms (Shanghai, China). The *GPR37*$^{-/-}$ mice (B6.129P2-Gpr37tm1Dgen/J), originally obtained from the Jackson Laboratory (http://jaxmice.jax.org/strain/005806.html), were provided by E. Peles from Weizmann Institute of Science, maintained on a C57BL/6J background, and genotyped as described previously (*40*). Olig2-cre mice were provided by B. Xiao from Southern University of Science and Technology. GPR37$^{loxP/loxP}$ mice were crossed with Olig2-cre$^{+/-}$ mice to generate GPR37 cKO (GPR37$^{loxP/loxP}$; Olig2-cre$^{+/-}$) and heterozygous (GPR37$^{loxP/+}$; Olig2-cre$^{+/-}$) mice. The *OCN*$^{-/-}$ line was genotyped using primers 5′-CCAAATCCCCTTGGCTTCTGACTG-3′ and 5′-ATCACCACCACGATGGACAGACTCGA-3′. The GPR37$^{loxP/loxP}$ line was genotyped using primers 5′-AGTTTTGTTGTTATGTCTGGTG-3′ and 5′-TGGAGATGAAAAGAGTGTCA-3′. The Olig2-Cre line was identified with the primers 5′-TGCCACGCACAAGTGACAGCAATG-3′ and 5′-ACCAGAGACGGAAATCCATCGCTC-3′.

Six- to 10-week-old mice, both male and female, were used interchangeably for experiments. For exogenous OCN treatment, the synthesized mouse OCN (100 ng/day) or phosphate-buffered saline (PBS) was delivered via ICV infusion for 10 days before experimental analysis. For rescues of function in *GPR37*$^{-/-}$ mice, high-titer lentivirus-containing mouse *GPR37* gene was delivered via ICV infusions before experimental analysis. To block OCN activity, OCN antibody (200 ng; Santa Cruz Biotechnology, sc-365797) and mouse IgG were infused via ICV before experimental analysis. Unless specified otherwise, statistical analyses were performed using two-tailed Student's *t* test.

EM analysis

The procedure for EM was performed as described previously with modifications (*64*). Briefly, mice were anesthetized and perfused with 15 ml of cacodylate (Sigma-Aldrich, St. Louis, USA) buffer (0.15 M, pH 7.4) followed by 30 ml of fixative mixture containing 0.08 M cacodylate (pH 7.4), 2.5% paraformaldehyde (PFA) (Sigma-Aldrich), 1.25% glutaraldehyde (Sigma-Aldrich), and 2 mM calcium chloride (Sigma-Aldrich). The brain and SC were carefully removed to avoid mechanical irritation and postfixed for 12 to 24 hours at 4°C in the fixative mixture. Then, tissues were first immersed in 1% (w/v) OsO_4 and 1.5% (w/v) potassium ferricyanide aqueous solution at 4°C for 2 hours. After washing, tissues were dehydrated through graded alcohol (30, 50, 70, 80, 90, 100%, 10 min each) into pure acetone (2 × 10 min). Samples were infiltrated in graded mixture (3:1, 1:1, and 1:3) of acetone and SPI-PON812 resin [19.6 ml of SPI-PON812, 6.6 ml of DDSA (Dodecenylsuccinic anhydride), and 13.8 ml of NMA (Methyl Nadic anhydride)] and then changed pure resin. Last, tissues were embedded in pure resin with 1.5% BDMA (Benzyldimethylamine) and polymerized for 12 hours at 45°C and 48 hours at 60°C. The ultrathin sections (70 nm thick) were sectioned with microtome (Leica EM UC6), double-stained by uranyl acetate and lead citrate, and examined by a transmission electron microscope (TEM) (FEI Tecnai Spirit120kV). A total number of 20 fields per section were randomly chosen to quantify the relative thickness of the myelin sheath by *g* ratio, which is defined as the ratio between the axonal diameter and the total fiber diameter. The severity of less tight myelin compactness was defined by dividing the number of split myelin sheath to the number of total myelin sheath in each EM image.

Immunofluorescence staining and confocal microscopy

For immunostaining, antibodies against MBP (BioLegend; 1:500), PLP1 (Abcam; 1:500), Oligo2 (Merck Millipore; 1:1000), CC1

(Merck Millipore; 1:500), PDGFRα (Cell Signaling Technology; 1:500), Flag (Sigma-Aldrich; 1:500), and GPR37 (Abcam; 1:500) were used. The following procedures were modified for a previous study (*47*), and mice at defined ages were deeply anesthetized and perfused with ice-cold PBS followed by 4% PFA. The brain and SC were dissected, fixed in 4% PFA overnight, dehydrated in 30% sucrose at 4°C, embedded in OCT (optimal cutting temperature compound) (Sakura Finetek), and processed for cryosections at 20 μm. For immunohistochemistry, cryosections were permeabilized and blocked in blocking buffer [0.4% Triton X-100 and 5% normal bovine serum albumin (BSA) in PBS] for 1 hour at room temperature and overnight with primary antibodies overnight at 4°C. After washing with PBS, sections were incubated with secondary antibodies labeled with Alexa Fluor 488 or 594 (Jackson ImmunoResearch Laboratories; 1:1000) for 1 hour at room temperature, stained with 4′,6-diamidino-2-phenylindole (DAPI) for 10 min, washed three times in PBS, and then mounted in Mounting Medium. For immunocytochemistry, cells were seeded on poly-L-lysine–coated glass coverslips at a density of 1×10^4 per well in the presence of ciliary neurotrophic factor (CNTF) and T3, and cells were treated with OCN before assessment. Briefly, cells were washed by PBS, fixed by 4% PFA, and then permeabilized at room temperature in 5% BSA for 1.5 hours followed by 0.3% Triton X-100 for 10 min. After that, cells were treated with primary antibodies overnight at 4°C. Secondary antibodies labeled with Alexa Fluor 488 or 594 were subsequently added to the cells. Last, coverslips were mounted on glass slides and imaged using a confocal microscope (LSM 880, Zeiss). Experiments were independently repeated at least three times.

BrdU assay

For proliferation assay in vivo, the $OCN^{-/-}$ mice were intraperitoneally injected with BrdU (100 μg/g body weight) (Sigma Aldrich) 2 days before sacrifice, and the BrdU-labeled cells were stained with anti-BrdU (Abcam; 1:500) antibody. For differentiation assay in vivo, mice were pulsed with BrdU (200 μg/g) at the beginning of treatment for four consecutive days, and the coimmunostaining of BrdU and CC1 was performed at the end of experiment.

Extraction of CSF and serum and measurement of OCN concentration

Collection of CSF from the cisterna magna was performed as previously described (*65*). Briefly, the mice were anesthetized by 1% pentobarbital sodium and then placed in a stereotaxic device. The skin of the neck was shaved, and the surgical site was swabbed with 10% povidone iodine, followed by 70% ethanol. A sagittal incision of the skin was made inferior to the occiput, and the subcutaneous tissue and muscles were separated under the dissection microscope. After the CSF space was visible, a glass capillary tube was inserted into the cisterna magna, and then the CSF was collected and stored at −80°C until use. For serum extraction, the whole-blood samples were collected from the mice and then centrifuged at 3000*g* for 10 min at 4°C, and the resulting serum was stored at −80°C until use. Contents of OCN in CSF and serum were measured using a mouse OCN ELISA kit (Cloud-Clone Corp., catalog no. SEA471Mu) according to the manufacturer's protocol.

LPC-induced demyelinating injury

LPC-induced demyelination was carried out in the CC and SC of 8-week-old WT and $OCN^{-/-}$ mice as described previously (*47*, *48*). Briefly, for CC injury, 1.5 μl of 1% (w/v) LPC (Sigma-Aldrich) in 0.9% NaCl was stereotactically injected into CC after exposing the skull. The coordinates were as follows: 1 mm backward to bregma, 1 mm lateral to bregma, and 1.5 mm deep relative to the skull surface. For SC injury, the spinal vertebrae at the level of T3 to T4 were exposed, and then meningeal tissue in the intervertebral space was cleared. After the dura was pierced, 0.5 μl of 1% (w/v) LPC was injected via a Hamilton syringe attached to a glass micropipette into the ventrolateral white matter via a stereotactic instrument. Brain and SC tissues carrying the lesions were harvested at different time points after LPC injection.

RNA-seq and data analysis

RNA was extracted from CC of WT and $OCN^{-/-}$ mice using TRIeasy Total RNA Extraction Reagent (YEASEN Biotechnology Co., Shanghai, China) and subjected to DNBSEQ sequencing platform by Beijing Genomics Institute (BGI; Wuhan, China). At least 40 million clean reads of sequencing depth were collected for each sample. RNA-seq raw data were initially filtered to obtain clean data after quality control, and the clean data were aligned to the mouse genome (mm10) by HISAT and Bowtie2. A highly optimized read count program called featureCounts was used to quantify reads generated from RNA-seq. Raw counts of each library were used to the R package DEseq2 for analysis of DEGs with false discovery rate < 0.05 (*66*). The raw data from RNA-seq experiments have been uploaded to the National Center for Biotechnology Information (NCBI) under the accession number GSE.

In situ hybridization

RNA in situ hybridization was carried out as previously described with slight modifications (*67*). $GPR37^{-/-}$ and their littermate WT mice were deeply anesthetized and perfused with PBS followed by 4% PFA. The SCs were dissected, postfixed in 4% PFA, cryoprotected in 20% sucrose overnight at 4°C, and then immersed in OCT Compound (Sakura Finetek) for subsequent sectioning. Tissue sections (20 μm) mounted on microscope slides were hybridized with digoxigenin (DIG)–labeled probe overnight at 56°C in a humidified and sealed container. The DIG-labeled complementary RNA (cRNA) probes were generated by in vitro transcription from an 838–base pair fragment of GPR37 with T7 RNA polymerase. The cRNA probes were diluted with hybridization buffer (1:1000) and denatured at 75°C before use. To reduce nonspecific binding of cRNA probes, sections were preincubated with hybridization buffer [5 × Denhardt's solution, baker's yeast transfer RNA (3 mg/ml), sheared herring sperm DNA (5 mg/ml), 5× SSC, and 50% formamide in ddH_2O] for at least 2 hours at room temperature. After overnight hybridization, slides were rinsed in wash buffer (1× SSC, 50% formamide, and 0.1% Tween-20) at 65°C for 2 × 20 min and then incubated in blocking solution (10% heat-inactivated sheep serum) for 1 hour at room temperature. After that, the tissue sections were incubated with anti-DIG–POD (peroxidase) antibody for 1 hour at 37°C, and the color reaction was performed using a TSA Plus Cy3 kit according to the manufacturer's instruction before the coverslips were subjected for confocal microscopy imaging (Zeiss LSM 880).

Viral vector construction

Lentiviral vectors inserting shRNA scramble or shRNA against rat GPR37 (gene ID: 117549) or GPR37L1 (gene ID: 252939) were constructed on the basis of the pLL3.7 plasmid (Addgene, #11795). The shRNA sequences were prepared by two primer annealing sites: 1#shGPR37, 5′-TCCAACGTCCAGATGTACTACCACACCTA

GTACATCTGGACGTTGGTTTTTTC-3′ (sense) and 5′-TCGAGAAAA AACCAACGTCCAGATGTACTAGGTGTGGTAGTACATCTG-GACGTTGGA-3′ (antisense); 2#shGPR37, 5′-TGGTTCCCATTA-C A G G C C T T C C A C A C C A A G G C C T G T A A T G G - GAACCTTTTTTC-3′ (sense) and 5′-TCGAGAAAAAAGGT TCCCATTACAGGCCTTGGTGTGGAAGGCCTGTAATGG-GAACCA-3′ (antisense); 3#shGPR37, 5′-TGCTTATCTGTGGT-G A T C T T C C A C A C C A A G A T C A C C A C A G A T A - AGCTTTTTTC-3′ (sense) and 5′-TCGAGAAAAAAGCTTATCTG TGGTGATCTTGGTGTGGAAGATCACCACAGATAAGCA-3′ (antisense); 1#shGPR37L1, 5′-TGGCACAGCTACTACTTGAAC-CACACCTTCAAGTAGTAGCTGTGCCTTTTTTC-3′ (sense) and 5′-TCGAGAAAAAAGGCACAGCTACTACTTGAAGGT-GTGGTTCAAGTAGTAGCTGTGCCA-3′ (antisense); 2#shGPR37L1, 5′-TGGGCATAGACCGATTCCATCCACACCATGGAATCG-GTCTATGCCCTTTTTTC-3′ (sense) and 5′-TCGAGAAAAAAG-GGCATAGACCGATTCCATGGTGTGGATGGAATCGGTC-TATGCCCA-3′ (antisense).

For GPR37-overexpressing vectors, full complementary DNA (cDNA) sequence of mouse GPR37 (gene ID: 14763) was amplified by reverse transcription PCR and cloned into lentiviral vector pUltra-Smurf (Addgene, #48974) at Age I and Eco RI restriction enzyme sites. The primers used for amplification were as follows: 5′-GTC-CGATCCACCGGTATGCCAGCCCGGGGCGCGCC-3′ (forward) and 5′-ACGAAGTTATGAATTTCAGCAATGAGTCCCCACAG-3′ (reverse). All the constructs were confirmed by DNA sequencing.

Transfection and lentivirus production

All transfections were performed with an optimized calcium phosphate method (*68*). Transfection efficiency was tested by real-time PCR or Western blot. High-titer lentiviruses were generated by transfecting HEK293T cells with the lentiviral vectors and two packaging plasmids including pVSVg (Addgene #8454) and psPAX2 (Addgene #12260), as described previously (*69*).

Intracellular calcium level measurement

The change of cytoplasmic free calcium ion concentration (iCa^{2+}) was determined on the basis of HEK293-GCaMP6s cells, i.e., a HEK293 cell line stably expressing GCaMP6s. (*70*). After 48 hours of transfection with GPR37 or GPR37L1 vectors in HEK293-GCaMP6s cells, the medium was exchanged by Hanks' balanced salt solution (HBSS; HBSS buffer, with Ca^{2+} and Mg^{2+}, Thermo Fisher Scientific, #14025092). Cells were incubated at 37°C for 30 min and then treated with OCN (20 nM). The iCa^{2+} level was reflected by the change of GCaMP6s fluorescent signals recorded using a Nikon digital imaging system (interval time of 1 s). All the data were quantified and analyzed by MATLAB.

Standard β-arrestin recruitment assay

The β-arrestin recruitment assay was measured in HTLA cells (a HEK293 cell line stably expressing a tTA-dependent luciferase reporter and a β-arrestin2–TEV fusion protein) using a PRESTO-Tango (parallel receptorome expression and screening via transcriptional output, with transcriptional activation following arrestin translocation) system (*52*). Four vectors of GPRs were purchased from Addgene, including GPR37-Tango (#66355), GPR37L1-Tango (#66356), GPRC6A-Tango (#66386), and GPR158-Tango (#66332). HTLA cells expressing these vectors were seeded in poly-L-lysine–coated and rinsed 96-well white, clear-bottomed cell-culture plates (Greiner Bio-One). The following day, stimulation solutions with various concentrations of OCN were prepared in filter-sterilized assay buffer, and 40 μl was added to each well. The medium was removed 24 hours later from the wells, and ONE-Glo EX Reagent (40 μl per well; Promega) diluted 20-fold in assay buffer was added to each well. After incubation for 15 to 20 min at 20° to 25°C, the plate was counted in the Synergy H1 Hybrid Multi-Mode Reader (BioTek). Relative luminescence units (RLUs) were exported into Excel spreadsheets, and GraphPad Prism was used for analysis of data.

Binding assays

Binding assays were performed with modifications as previously described (*71*). Briefly, a 100-mm dish of HEK293T cells was transfected with 10 μg of the expression construct containing GPR37 or GPR37L1. After 36 hours of transfection, cells were dissociated with an enzyme-free cell-dissociation buffer (Life Technologies), washed with PBS, and plated on white CoStar 96-well plates pretreated with poly-L-lysine. For saturation binding assays and calculation of the dissociation constant, K_d, 24 hours later, cells were washed with binding medium (0.5% BSA in Ca^{2+}/Mg^{2+} PBS) and incubated with serial dilutions of biotinylated OCN in binding medium for 2 hours at 37°C. OCN biotinylation was performed using the Biotin Protein Labeling Kit (catalog no. 11418165001) from Roche. Following three times washes with binding medium, cells were fixed with 4% PFA for 10 min, washed with binding medium supplemented with 0.3% Triton X-100, and further incubated for 30 min with extra-avidin peroxidase (Sigma-Aldrich) in binding buffer. Cells were extensively washed, and bound peroxidase was quantified using trimethylboron (TMB) substrate (Thermo Fisher Scientific). The reaction was terminated by addition of TMB stop solution (Immunochemistry Technologies), and absorbance was read at 450 nm in an Infinite M200Pro (Tecan) microplate reader. Nonspecific binding was determined in the presence of 100 μM nonbiotinylated OCN, and specific binding was calculated by subtracting absorbance values for nonspecific binding from total binding values. Control experiments were performed using the maximum amount of biotinylated protein and HEK293T cells transiently transfected with the pcDNA3.1 vector alone, but no signal was detected.

Pulldown assay

Pulldown assay was performed in solubilized membranes from HEK293 cells overexpressing GPR37 or GPR37L1. After 48 hours of transfection with FLAG-GPR37 and FLAG-GPR37L1 vectors, cells were homogenized on ice with cell lysis buffer [10 mM tris-HCl (pH 7.4), 320 mM sucrose, 1× protease, and phosphatase inhibitor cocktail (78443; Thermo Fisher Scientific)]. Homogenization was centrifuged at 12,000*g* for 15 min at 4°C. Then, supernatants were collected and incubated with anti-FLAG (F1804, Sigma-Aldrich) overnight at 4°C. After that, 20 μl of Protein A/G PLUS-Agarose (sc-2003; Santa Cruz Biotechnology) was added for 2 hours at room temperature followed by three washes with 1× PBS. Mouse OCN was biotinylated using the Biotin Protein Labeling Kit (catalog no. 11418165001, Roche) according to the manufacturer's instructions. For the pulldown, biotinylated OCN (5 μg) was added and incubated for 1 hour at 4°C. Purified proteins were eluted from the beads by adding Laemmli protein buffer and heated at 65°C for 15 min and analyzed by Western blot.

Cell culture and treatment

Cell lines including HEK293T, HEK-GCaMP6s, and HTLA cells were routinely cultured in Dulbecco's modified Eagle's medium

(DMEM) supplemented with 10% fetal bovine serum, penicillin (100 U/ml), and streptomycin (100 μg/ml) [for HTLA cells, with additional puromycin (2 μg/ml) and hygromycin B (100 μg/ml)] at 37°C in a humidified incubator with 5% CO_2. The HEK293T cells were originally obtained from the American Type Culture Collection, and HEK-GCaMP6s cells were generated by infecting HEK293T cells with lentivirus containing GCaMP6s.

Primary rat OPCs were isolated and cultured as described previously (*46*). The forebrains were dissected from P1 or P2 Sprague-Dawley rat pups, and meninges were removed and discarded. The cerebral cortex was isolated and then transferred to a 1.5-ml Eppendorf tube. The tissues were homogenized by pipetting up and down with mixed culture growth medium, consisting of DMEM-F12 (Gibco, catalog no. 11330-032), 10% fetal bovine serum (Gibco, catalog no. 10270-106), and penicillin (100 U/ml)/streptomycin (100 g/ml). Cell suspension was passed through a 40-μm cell strainer (Falcon; catalog no. 352340) and seeded in poly-L-lysine–precoated (Sigma-Aldrich, P0899; 0.1 mg/ml in PBS) T75 flasks. The cells were cultured at 37°C in a humidified incubator with 5% CO_2/95% air for up to 12 days, with the medium changed every 3 days. After that, microglia was aspirated off with the medium by shaking the flasks at 37°C, 200 rpm for 1 hour, then replaced with fresh growth medium, and shaken overnight with caps tightly closed for 19 hours. Cell suspension was plated onto 10-cm dish for 4 to 6 hours at 37°C with 5% CO_2, and the medium was replaced by Knockout DMEM-F12 medium (Gibco, catalog no. 12660012) supplemented with B27 Supplement (Gibco, catalog no. A3582801), Neural Supplement (Life Technologies, catalog no. A1050801), N2 supplement (Gibco, catalog no. A1370701), sodium pyruvate (Gibco, catalog no. 11360070), GlutaMax supplement (Gibco, catalog no. 35050061), penicillin/streptomycin, PDGF-AA (PeproTech, catalog no. 100-13A), human basic fibroblast growth factor (Sino Biological, catalog no. 10014HNAE), insulin (Sigma-Aldrich, catalog no. 91077), *N*-acetyl cysteine (Sigma-Aldrich, catalog no. A8199), and epidermal growth factor. The differentiation of OPC into mature OLs was induced by adding CNTF (PeproTech, catalog no. 450-13) and T3 (Sigma-Aldrich, catalog no. T6397) into the culture medium. Primary mouse OPCs were isolated from P7 to P8 *GPR37*$^{-/-}$ mice as described previously (*72*, *73*). Mouse OPC induced differentiation into mature OLs by T3 (Sigma-Aldrich, catalog no. T2877) and CNTF as described above. The purity of OPC and induction to OLs were assessed by specific markers. To examine function of OCN in OLs, rat OPCs were transduced with the lentiviral vector carrying shRNA targeting GPR37 or GPR37L1 and differentiated in the presence of CNTF and T3 for 48 hours before subsequent analyses. OLs derived from primary rat OPCs were treated with OCN or TX14(A) in differentiation medium for 48 hours before subsequent experiments. To restore the GPR37 level, differentiation OLs were infected with lentivirus containing mouse GPR37 for 48 hours before subsequent OCN treatment.

Peptide

Human and mouse OCN peptides were synthesized in the BGI (Beijing, China). The complete amino acid sequence is as follows: for human OCN, YLYQWLGAPVPYPDPLEPRREVCELNPDCD ELADHIGFQEAYRRFYGPV; for mouse OCN, YLGASVPSPD-PLEPTREQCELNPACDELSDQYGLKTAYKRIYGITI. Prosaptide TX14 (A) was purchased from Sigma-Aldrich (catalog no. SML1417). All the peptides were dissolved in PBS and stored at −80°C until use.

cAMP production assays

For cAMP measurement in HEK293, after the transfection of GPR37 or GPR37L1 vectors for 48 hours, cells were seeded in poly-L-lysine–coated and rinsed 96-well white, clear-bottomed cell-culture plates (Greiner Bio-One). By the treatment with forskolin and/or various amounts of OCN for 30 min, the cAMP level was analyzed using the cAMP-Glo Max Assay Kit (Promega, catalog no. V1682) following the manufacturer's instructions.

For cAMP quantification in OL, primary rat OPCs were transduced with the lentiviral vector carrying shRNA targeting GPR37 in the presence of CNTF and T3 for 48 hours and then seeded in poly-L-lysine–coated wells of 96-well plates at a density of 1×10^4 per well. Cells were treated with forskolin and OCN at the indicated concentration for 30 min, and the intracellular cAMP concentration was measured with the same kit as described above. All the experiments were repeated at least four times in triplicate, and data were analyzed using GraphPad Prism software.

Cell proliferation and cell viability

For cell proliferation assay, primary rat OPCs were seeded in poly-L-lysine–coated 96-well plates at a density of 1×10^4/well and treated with OCN (20 nM) before assessment. Cell proliferation was measured using EdU (5-ethynyl-2'-deoxyuridine) incorporation assay (RiboBio, Guangzhou, China) according to the instructions of the manufacturer.

For cell viability measurement, primary rat OPCs were seeded in poly-L-lysine–coated 96-well plates at a density of 1×10^4 per well in the presence of CNTF and T3, and cells were treated with OCN in different concentrations (from 0 to 50 nM) or times (up to 72 hours) before assessment. Cell viability assay was measured using an MTT [3-(4,5)-dimethylthiahiazo (-z-y1)-3,5-di-phenytetrazoliumromide] kit (Beyotime, China) according to the instructions of the manufacturer.

Western blotting

Total proteins were extracted with radioimmunoprecipitation assay buffer [20 mM tris-HCl (pH 7.5), 150 mM NaCl, 1 mM EDTA, 1% Triton X-100, 0.5% sodium deoxycholate, and 1 mM phenylmethylsulfonyl fluoride] supplemented with protease inhibitor cocktail (Roche). Protein concentration of samples was measured using a bicinchoninic acid protein assay kit (Thermo Fisher Scientific). Equal protein amounts (30 to 50 μg) were loaded for SDS-PAGE and transferred to a polyvinylidene difluoride or nitrocellulose membrane. After blocking the nonspecific site with 5% nonfat milk for 1 hour, the membrane was incubated with a specific primary antibody overnight at 4°C and then incubated with horseradish peroxidase–conjugated secondary antibody for 1 hour at room temperature. The immune blotting signals were visualized with an enhanced chemiluminescence (ECL) kit (Thermo Fisher Scientific, catalog no. 32209) using a chemiluminescent imaging system (5200Multi, Tanon). Digital images were quantified using densitometric measurement with ImageJ software.

RNA extraction and quantitative reverse transcription PCR

Total RNA from cells or tissue was extracted using TRIzol Reagent (Invitrogen, Carlsbad, CA, USA) according to the manufacturer's instructions. The concentration of RNA was quantified by the NanoDrop 2000c Spectrophotometer (Thermo Fisher Scientific, Rockford, IL). The first-strand cDNA was synthesized from 1 μg of total RNA using One-Step gDNA Removal and cDNA Synthesis SuperMix (TransGen Biotech, Beijing, China). The quantitative PCR experiments were conducted on a QuantStudio Real-Time PCR system (Applied Biosystems)

using TransStart Tip Green qPCR SuperMix (TransGen Biotech) with gene-specific primers. Glyceraldehyde-3-phosphate dehydrogenase (GAPDH) was used as an internal control for normalization. Primer sequences used in this study were supplemented in table S1. All reactions were performed in triplicate with three independent experiments, and the relative expression of mRNA levels was calculated using the $2^{-\Delta\Delta Ct}$ method.

X-ray microscope analysis

The 3D imaging of SC was performed using the ZEISS Xradia 520 Versa X-ray Microscope [Carl Zeiss (Shanghai) Co. Ltd., Shanghai, China]. The specimens were stained with 1% osmium acid solution and dried with the critical point drying method. Before imaging, the specimens were mounted on the sample holder with an aluminum tube as adapter and rotated horizontally by 360°, pausing at discrete angles to collect 2D projection images, which were then combined together to produce a 3D reconstruction of the specimen's volume dataset. Scanning energy is 40 to 60 kV, and scanning resolution is from 0.5 to 2.0 μm/voxel size. The low resolutions are for the large filed of sample scanning, and fine resolutions are for the local high-resolution scanning. Each 3D dataset includes about 1000 virtual slices. The volume of 3D datasets is about 2 GB in CCD (Charge-coupled Device) bin2 mode. Dragonfly software from Object Research Systems (ORS) Inc. is hired for dataset processing. The 3D internal structure of SC is presented after segmentation and 3D rendering.

Behavioral tests in mice

Thermal sensitivity test

Thermal sensitivity was measured with a hot plate test apparatus (Bioseb in Vivo Research Instrument) in 8-week-old mice. The latency to respond to a thermal stimulus applied to the paws is determined by the time it takes the mouse to lick or flick the hind paw or jump from the hot plate surface. These reflexive behaviors involve both cerebral and spinal mediated circuits. The temperature of the hot plate is calibrated to produce a withdrawal response within 10 to 15 s in control mice. The surface temperature of the plate was controlled at 53°C. For the OCN rescue experiment, the $OCN^{-/-}$ mice were performed with hot plate test after intraperitoneal injection of the synthesized mouse OCN (50 ng/g, body weight) for 10 days.

Pupillary light reflex

Pupillary light reflex was recorded in 8-week-old mice with deep anesthesia. The pupil and corneal reflection was monitored by infrared light (780 nm), and the response of pupil was measured using a high-speed camera (3000f/s, Basler, acA1300—200 μm) focused on the anterior segment of the eye. Baseline pupil size was collected during the fixation period before the onset of white light stimulus. The pupil data were extracted by LabView software and analyzed by MATLAB.

Forelimb grip strength test

The test was performed with mice at 6 to 8 weeks of age by using the Grip Strength Meter (XR501, Shanghai Xinruan Information Technology Co. Ltd., Shanghai, China). Each mouse was lifted by the tail to grasp the bar mounted on the force gauge. Once both forelimbs gripped the bar, the mouse was then slowly pulled away from the meter by its tail at a constant speed until the forelimbs were released. The maximal forelimb force (in newton) was recorded by the gauge, and the measurement was performed three times for each mouse, which were finally averaged for the data analysis.

Open-field test

The open-field test was used to assess locomotor activity in mice at 6 to 8 weeks of age. Each mouse was placed in the center of a chamber (50 cm by 50 cm by 25 cm) and allowed to freely explore in the open field for 10 min. Spontaneous locomotor activity was recorded by an automated video tracking system. For analyses, a smaller concentric square covering 25% of the area (25 cm by 25 cm) was defined as the center area. The locomotion parameters including time in the center and total distance in the entire zone were analyzed by ANY-maze software (Stoelting Co.).

Statistical analysis

Statistical analyses were performed with the SPSS version 13.0 software 261 package (SPSS, Chicago, IL, USA) for Windows. All data are presented as means ± SD unless otherwise stated. When only two groups were compared, the statistical differences were assessed with the double-sided Student's *t* test. The number of samples per group ($n \geq 5$) is stated in the figure legends. Comparisons among multiple groups were performed using one-way analysis of variance (ANOVA) with Tukey's post hoc test. Two-way ANOVA was used for analysis of multiple groups with Tukey's multiple comparison post hoc test. For all experiments, $^*P \leq 0.05$ was considered a significant difference.

SUPPLEMENTARY MATERIALS

Supplementary material for this article is available at https://science.org/doi/10.1126/sciadv.abi5811

View/request a protocol for this paper from *Bio-protocol*.

REFERENCES AND NOTES

1. P. Ducy, C. Desbois, B. Boyce, G. Pinero, B. Story, C. Dunstan, E. Smith, J. Bonadio, S. Goldstein, C. Gundberg, A. Bradley, G. Karsenty, Increased bone formation in osteocalcin-deficient mice. *Nature* **382**, 448–452 (1996).
2. G. Karsenty, Update on the biology of osteocalcin. *Endocr. Pract.* **23**, 1270–1274 (2017).
3. A. Obri, L. Khrimian, G. Karsenty, F. Oury, Osteocalcin in the brain: From embryonic development to age-related decline in cognition. *Nat. Rev. Endocrinol.* **14**, 174–182 (2018).
4. G. Karsenty, E. N. Olson, Bone and muscle endocrine functions: Unexpected paradigms of inter-organ communication. *Cell* **164**, 1248–1256 (2016).
5. P. Mera, M. Ferron, I. Mosialou, Regulation of energy metabolism by bone-derived hormones. *Cold Spring Harb. Perspect. Med.* **8**, a031666 (2018).
6. N. K. Lee, H. Sowa, E. Hinoi, M. Ferron, J. D. Ahn, C. Confavreux, R. Dacquin, P. J. Mee, M. D. McKee, D. Y. Jung, Z. Zhang, J. K. Kim, F. Mauvais-Jarvis, P. Ducy, G. Karsenty, Endocrine regulation of energy metabolism by the skeleton. *Cell* **130**, 456–469 (2007).
7. T. C. Brennan-Speranza, A. D. Conigrave, Osteocalcin: An osteoblast-derived polypeptide hormone that modulates whole body energy metabolism. *Calcif. Tissue Int.* **96**, 1–10 (2015).
8. F. Oury, G. Sumara, O. Sumara, M. Ferron, H. Chang, C. E. Smith, L. Hermo, S. Suarez, B. L. Roth, P. Ducy, G. Karsenty, Endocrine regulation of male fertility by the skeleton. *Cell* **144**, 796–809 (2011).
9. F. Oury, M. Ferron, W. Huizhen, C. Confavreux, L. Xu, J. Lacombe, P. Srinivas, A. Chamouni, F. Lugani, H. Lejeune, T. R. Kumar, I. Plotton, G. Karsenty, Osteocalcin regulates murine and human fertility through a pancreas-bone-testis axis. *J. Clin. Invest.* **123**, 2421–2433 (2013).
10. M. Ferron, J. Wei, T. Yoshizawa, A. del Fattore, R. A. DePinho, A. Teti, P. Ducy, G. Karsenty, Insulin signaling in osteoblasts integrates bone remodeling and energy metabolism. *Cell* **142**, 296–308 (2010).
11. K. Kover, Y. Yan, P. Y. Tong, D. Watkins, X. Li, J. Tasch, M. Hager, M. Clements, W. V. Moore, Osteocalcin protects pancreatic beta cell function and survival under high glucose conditions. *Biochem. Biophys. Res. Commun.* **462**, 21–26 (2015).
12. M. Ferron, E. Hinoi, G. Karsenty, P. Ducy, Osteocalcin differentially regulates beta cell and adipocyte gene expression and affects the development of metabolic diseases in wild-type mice. *Proc. Natl. Acad. Sci. U.S.A.* **105**, 5266–5270 (2008).
13. P. Mera, K. Laue, M. Ferron, C. Confavreux, J. Wei, M. Galán-Díez, A. Lacampagne, S. J. Mitchell, J. A. Mattison, Y. Chen, J. Bacchetta, P. Szulc, R. N. Kitsis, R. de Cabo,

R. A. Friedman, C. Torsitano, T. E. McGraw, M. Puchowicz, I. Kurland, G. Karsenty, Osteocalcin signaling in myofibers is necessary and sufficient for optimum adaptation to exercise. *Cell Metab.* **23**, 1078–1092 (2016).
14. P. Mera, K. Laue, J. Wei, J. M. Berger, G. Karsenty, Osteocalcin is necessary and sufficient to maintain muscle mass in older mice. *Mol. Metab.* **5**, 1042–1047 (2016).
15. C. Greenhill, Bone: Osteocalcin influences fetal brain development and adult brain function. *Nat. Rev. Endocrinol.* **9**, 689 (2013).
16. F. Oury, L. Khrimian, C. A. Denny, A. Gardin, A. Chamouni, N. Goeden, Y.-y. Huang, H. Lee, P. Srinivas, X.-B. Gao, S. Suyama, T. Langer, J. J. Mann, T. L. Horvath, A. Bonnin, G. Karsenty, Maternal and offspring pools of osteocalcin influence brain development and functions. *Cell* **155**, 228–241 (2013).
17. A. Chamouni, C. Schreiweis, F. Oury, Bone, brain & beyond. *Rev. Endocr. Metab. Disord.* **16**, 99–113 (2015).
18. C. Shan, A. Ghosh, X.-z. Guo, S.-m. Wang, Y.-f. Hou, S.-t. Li, J.-m. Liu, Roles for osteocalcin in brain signalling: Implications in cognition- and motor-related disorders. *Mol. Brain* **12**, 23 (2019).
19. M. Pi, K. Kapoor, R. Ye, S. K. Nishimoto, J. C. Smith, J. Baudry, L. D. Quarles, Evidence for osteocalcin binding and activation of GPRC6A in β-cells. *Endocrinology* **157**, 1866–1880 (2016).
20. J. Wei, T. Hanna, N. Suda, G. Karsenty, P. Ducy, Osteocalcin promotes β-cell proliferation during development and adulthood through Gprc6a. *Diabetes* **63**, 1021–1031 (2014).
21. M. Pi, L. D. Quarles, Multiligand specificity and wide tissue expression of GPRC6A reveals new endocrine networks. *Endocrinology* **153**, 2062–2069 (2012).
22. L. Khrimian, A. Obri, M. Ramos-Brossier, A. Rousseaud, S. Moriceau, A.-S. Nicot, P. Mera, S. Kosmidis, T. Karnavas, F. Saudou, X.-B. Gao, F. Oury, E. Kandel, G. Karsenty, Gpr158 mediates osteocalcin's regulation of cognition. *J. Exp. Med.* **214**, 2859–2873 (2017).
23. D. E. Bergles, W. D. Richardson, Oligodendrocyte development and plasticity. *Cold Spring Harb. Perspect. Biol.* **8**, a020453 (2015).
24. T. Philips, J. D. Rothstein, Oligodendroglia: Metabolic supporters of neurons. *J. Clin. Invest.* **127**, 3271–3280 (2017).
25. K. A. Nave, H. B. Werner, Myelination of the nervous system: Mechanisms and functions. *Annu. Rev. Cell Dev. Biol.* **30**, 503–533 (2014).
26. A. S. Saab, K. A. Nave, Myelin dynamics: Protecting and shaping neuronal functions. *Curr. Opin. Neurobiol.* **47**, 104–112 (2017).
27. X. Zhao, X. He, X. Han, Y. Yu, F. Ye, Y. Chen, T. Hoang, X. Xu, Q.-S. Mi, M. Xin, F. Wang, B. Appel, Q. R. Lu, MicroRNA-mediated control of oligodendrocyte differentiation. *Neuron* **65**, 612–626 (2010).
28. S. Moyon, P. Casaccia, DNA methylation in oligodendroglial cells during developmental myelination and in disease. *Neurogenesis (Austin, Tex.)* **4**, e1270381 (2017).
29. S. Mitew, C. M. Hay, H. Peckham, J. Xiao, M. Koenning, B. Emery, Mechanisms regulating the development of oligodendrocytes and central nervous system myelin. *Neuroscience* **276**, 29–47 (2014).
30. H. Li, W. D. Richardson, Genetics meets epigenetics: HDACs and Wnt signaling in myelin development and regeneration. *Nat. Neurosci.* **12**, 815–817 (2009).
31. Y. Chen, H. Wu, S. Wang, H. Koito, J. Li, F. Ye, J. Hoang, S. S. Escobar, A. Gow, H. A. Arnett, B. D. Trapp, N. J. Karandikar, J. Hsieh, Q. R. Lu, The oligodendrocyte-specific G protein-coupled receptor GPR17 is a cell-intrinsic timer of myelination. *Nat. Neurosci.* **12**, 1398–1406 (2009).
32. K. M. Young, K. Psachoulia, R. B. Tripathi, S.-J. Dunn, L. Cossell, D. Attwell, K. Tohyama, W. D. Richardson, Oligodendrocyte dynamics in the healthy adult CNS: Evidence for myelin remodeling. *Neuron* **77**, 873–885 (2013).
33. K. A. Nave, H. Ehrenreich, Myelination and oligodendrocyte functions in psychiatric diseases. *JAMA Psychiat.* **71**, 582–584 (2014).
34. R. J. M. Franklin, C. Ffrench-Constant, Regenerating CNS myelin—From mechanisms to experimental medicines. *Nat. Rev. Neurosci.* **18**, 753–769 (2017).
35. R. Takahashi, Y. Imai, Pael receptor, endoplasmic reticulum stress, and Parkinson's disease. *J. Neurol.* **250** Suppl. 3, iii25–iii29 (2003).
36. D. Marazziti, S. Mandillo, C. di Pietro, E. Golini, R. Matteoni, G. P. Tocchini-Valentini, GPR37 associates with the dopamine transporter to modulate dopamine uptake and behavioral responses to dopaminergic drugs. *Proc. Natl. Acad. Sci. U.S.A.* **104**, 9846–9851 (2007).
37. Y. Imai, M. Soda, H. Inoue, N. Hattori, Y. Mizuno, R. Takahashi, An unfolded putative transmembrane polypeptide, which can lead to endoplasmic reticulum stress, is a substrate of Parkin. *Cell* **105**, 891–902 (2001).
38. D. Marazziti, E. Golini, S. Mandillo, A. Magrelli, W. Witke, R. Matteoni, G. P. Tocchini-Valentini, Altered dopamine signaling and MPTP resistance in mice lacking the Parkinson's disease-associated GPR37/parkin-associated endothelin-like receptor. *Proc. Natl. Acad. Sci. U.S.A.* **101**, 10189–10194 (2004).
39. Y. Zhang, K. Chen, S. A. Sloan, M. L. Bennett, A. R. Scholze, S. O'Keeffe, H. P. Phatnani, P. Guarnieri, C. Caneda, N. Ruderisch, S. Deng, S. A. Liddelow, C. Zhang, R. Daneman, T. Maniatis, B. A. Barres, J. Q. Wu, An RNA-sequencing transcriptome and splicing database of glia, neurons, and vascular cells of the cerebral cortex. *J. Neurosci.* **34**, 11929–11947 (2014).
40. H.-J. Yang, A. Vainshtein, G. Maik-Rachline, E. Peles, G protein-coupled receptor 37 is a negative regulator of oligodendrocyte differentiation and myelination. *Nat. Commun.* **7**, 10884 (2016).
41. X. Morato, R. Luján, M. López-Cano, J. Gandía, I. Stagljar, M. Watanabe, R. A. Cunha, V. Fernández-Dueñas, F. Ciruela, The Parkinson's disease-associated GPR37 receptor interacts with striatal adenosine A_{2A} receptor controlling its cell surface expression and function in vivo. *Sci. Rep.* **7**, 9452 (2017).
42. S. Bang, Y.-K. Xie, Z.-J. Zhang, Z. Wang, Z.-Z. Xu, R.-R. Ji, GPR37 regulates macrophage phagocytosis and resolution of inflammatory pain. *J. Clin. Invest.* **128**, 3568–3582 (2018).
43. R. C. Meyer, M. M. Giddens, S. A. Schaefer, R. A. Hall, GPR37 and GPR37L1 are receptors for the neuroprotective and glioprotective factors prosaptide and prosaposin. *Proc. Natl. Acad. Sci. U.S.A.* **110**, 9529–9534 (2013).
44. B. Liu, V. Mosienko, B. Vaccari Cardoso, D. Prokudina, M. Huentelman, A. G. Teschemacher, S. Kasparov, Glio- and neuro-protection by prosaposin is mediated by orphan G-protein coupled receptors GPR37L1 and GPR37. *Glia* **66**, 2414–2426 (2018).
45. O. Jahn, S. Tenzer, H. B. Werner, Myelin proteomics: Molecular anatomy of an insulating sheath. *Mol. Neurobiol.* **40**, 55–72 (2009).
46. Y. Chen, V. Balasubramaniyan, J. Peng, E. C. Hurlock, M. Tallquist, J. Li, Q. R. Lu, Isolation and culture of rat and mouse oligodendrocyte precursor cells. *Nat. Protoc.* **2**, 1044–1051 (2007).
47. Z. Liu, M. Yan, Y. Liang, M. Liu, K. Zhang, D. Shao, R. Jiang, L. Li, C. Wang, D. R. Nussenzveig, K. Zhang, S. Chen, C. Zhong, W. Mo, B. M. A. Fontoura, L. Zhang, Nucleoporin Seh1 interacts with Olig2/Brd7 to promote oligodendrocyte differentiation and myelination. *Neuron* **102**, 587–601 e587 (2019).
48. J. Wang, L. Yang, C. Dong, J. Wang, L. Xu, Y. Qiu, Q. Weng, C. Zhao, M. Xin, Q. R. Lu, EED-mediated histone methylation is critical for CNS myelination and remyelination by inhibiting WNT, BMP, and senescence pathways. *Sci. Adv.* **6**, eaaz6477 (2020).
49. A. Mogha, M. D'Rozario, K. R. Monk, G protein-coupled receptors in myelinating glia. *Trends Pharmacol. Sci.* **37**, 977–987 (2016).
50. N. J. Smith, Drug discovery opportunities at the endothelin B receptor-related orphan G protein-coupled receptors, GPR37 and GPR37L1. *Front. Pharmacol.* **6**, 275 (2015).
51. S. Kosmidis, A. Polyzos, L. Harvey, M. Youssef, C. A. Denny, A. Dranovsky, E. R. Kandel, RbAp48 protein is a critical component of GPR158/OCN signaling and ameliorates age-related memory loss. *Cell Rep.* **25**, 959–973.e6 (2018).
52. W. K. Kroeze, M. F. Sassano, X.-P. Huang, K. Lansu, J. D. McCorvy, P. M. Giguère, N. Sciaky, B. L. Roth, PRESTO-Tango as an open-source resource for interrogation of the druggable human GPCRome. *Nat. Struct. Mol. Biol.* **22**, 362–369 (2015).
53. J. L. Salzer, B. Zalc, Myelination. *Curr. Biol.* **26**, R971–R975 (2016).
54. A. I. Basbaum, D. M. Bautista, G. Scherrer, D. Julius, Cellular and molecular mechanisms of pain. *Cell* **139**, 267–284 (2009).
55. R. Kardon, Pupillary light reflex. *Curr. Opin. Ophthalmol.* **6**, 20–26 (1995).
56. B. G. Brinkmann, A. Agarwal, M. W. Sereda, A. N. Garratt, T. Müller, H. Wende, R. M. Stassart, S. Nawaz, C. Humml, V. Velanac, K. Radyushkin, S. Goebbels, T. M. Fischer, R. J. Franklin, C. Lai, H. Ehrenreich, C. Birchmeier, M. H. Schwab, K. A. Nave, Neuregulin-1/ErbB signaling serves distinct functions in myelination of the peripheral and central nervous system. *Neuron* **59**, 581–595 (2008).
57. B. Emery, Q. R. Lu, Transcriptional and epigenetic regulation of oligodendrocyte development and myelination in the central nervous system. *Cold Spring Harb. Perspect. Biol.* **7**, a020461 (2015).
58. B. Emery, D. Agalliu, J. D. Cahoy, T. A. Watkins, J. C. Dugas, S. B. Mulinyawe, A. Ibrahim, K. L. Ligon, D. H. Rowitch, B. A. Barres, Myelin gene regulatory factor is a critical transcriptional regulator required for CNS myelination. *Cell* **138**, 172–185 (2009).
59. M. Koenning, S. Jackson, C. M. Hay, C. Faux, T. J. Kilpatrick, M. Willingham, B. Emery, Myelin gene regulatory factor is required for maintenance of myelin and mature oligodendrocyte identity in the adult CNS. *J. Neurosci.* **32**, 12528–12542 (2012).
60. S. Mandillo, E. Golini, D. Marazziti, C. di Pietro, R. Matteoni, G. P. Tocchini-Valentini, Mice lacking the Parkinson's related GPR37/PAEL receptor show non-motor behavioral phenotypes: Age and gender effect. *Genes Brain Behav.* **12**, 465–477 (2013).
61. M. S. Kaller, A. Lazari, C. Blanco-Duque, C. Sampaio-Baptista, H. Johansen-Berg, Myelin plasticity and behaviour-connecting the dots. *Curr. Opin. Neurobiol.* **47**, 86–92 (2017).
62. R. D. Fields, A new mechanism of nervous system plasticity: Activity-dependent myelination. *Nat. Rev. Neurosci.* **16**, 756–767 (2015).
63. M. N. Rasband, E. Peles, The nodes of Ranvier: Molecular assembly and maintenance. *Cold Spring Harb. Perspect. Biol.* **8**, (2016).
64. Y. Hua, P. Laserstein, M. Helmstaedter, Large-volume *en-bloc* staining for electron microscopy-based connectomics. *Nat. Commun.* **6**, 7923 (2015).

65. L. Liu, K. Duff, A technique for serial collection of cerebrospinal fluid from the cisterna magna in mouse. *J. Vis. Exp.* e960 (2008).
66. M. I. Love, W. Huber, S. Anders, Moderated estimation of fold change and dispersion for RNA-seq data with DESeq2. *Genome Biol.* **15**, 550 (2014).
67. N. P. Pringle, W.-P. Yu, M. Howell, J. S. Colvin, D. M. Ornitz, W. D. Richardson, Fgfr3 expression by astrocytes and their precursors: Evidence that astrocytes and oligodendrocytes originate in distinct neuroepithelial domains. *Development* **130**, 93–102 (2003).
68. M. Jordan, A. Schallhorn, F. M. Wurm, Transfecting mammalian cells: Optimization of critical parameters affecting calcium-phosphate precipitate formation. *Nucleic Acids Res.* **24**, 596–601 (1996).
69. T. Dittgen, A. Nimmerjahn, S. Komai, P. Licznerski, J. Waters, T. W. Margrie, F. Helmchen, W. Denk, M. Brecht, P. Osten, Lentivirus-based genetic manipulations of cortical neurons and their optical and electrophysiological monitoring in vivo. *Proc. Natl. Acad. Sci. U.S.A.* **101**, 18206–18211 (2004).
70. T. W. Chen, T. J. Wardill, Y. Sun, S. R. Pulver, S. L. Renninger, A. Baohan, E. R. Schreiter, R. A. Kerr, M. B. Orger, V. Jayaraman, L. L. Looger, K. Svoboda, D. S. Kim, Ultrasensitive fluorescent proteins for imaging neuronal activity. *Nature* **499**, 295–300 (2013).
71. I. Mosialou, S. Shikhel, J.-M. Liu, A. Maurizi, N. Luo, Z. He, Y. Huang, H. Zong, R. A. Friedman, J. Barasch, P. Lanzano, L. Deng, R. L. Leibel, M. Rubin, T. Nickolas, W. Chung, L. M. Zeltser, K. W. Williams, J. E. Pessin, S. Kousteni, MC4R-dependent suppression of appetite by bone-derived lipocalin 2. *Nature* **546**, 440 (2017).
72. Z. Ou, Y. Ma, Y. Sun, G. Zheng, S. Wang, R. Xing, X. Chen, Y. Han, J. Wang, Q. R. Lu, T.-J. Zhao, Y. Chen, A GPR17-cAMP-lactate signaling axis in oligodendrocytes regulates whole-body metabolism. *Cell Rep.* **26**, 2984–2997.e4 (2019).
73. J. R. Chan, T. A. Watkins, J. M. Cosgaya, C.-Z. Zhang, L. Chen, L. F. Reichardt, E. M. Shooter, B. A. Barres, NGF controls axonal receptivity to myelination by Schwann cells or oligodendrocytes. *Neuron* **43**, 183–191 (2004).

Acknowledgments: We are grateful to C. Peng and X. Li for helping with EM sample preparation and taking TEM images at the Center for Biological Imaging (CBI), Institute of Biophysics, and Chinese Academy of Sciences. We thank C. Cao [Carl Zeiss (Shanghai) Co. Ltd., Shanghai, China] for the assistance of 3D x-ray microscopy analysis. We appreciate Dr. Y. Li, Dr. Y. Wang, Dr. H. Kettenmann, and Dr. F. Xu for their comments on our manuscript before submission. **Funding:** This work was partially supported by Shenzhen Government Basic Research Program (JCYJ20170818164405101 and JCYJ20180508163203807), Guangdong Basic and Applied Basic Research Foundation (2019A1515012200), National Key R&D Program of China (2017YFC1310503), National Natural Science Foundation of China (91732304 and 31930047), Strategic Priority Research Program of Chinese Academy of Sciences (XDB32030100), CAS Key Laboratory of Brain Connectome and Manipulation (2019DP173024), Guangdong Provincial Key Laboratory of Brain Connectome and Behavior (2017B030301017), Guangdong Special Support Program, Key Laboratory of SIAT (2019DP173024), and Shenzhen Key Science and Technology Infrastructure Planning Project (ZDKJ20190204002). **Author contributions:** Z.Q. and X.L. conceived the study and designed all the experiments. Z.Q. and H.L. performed most of the experiments. H.Y. performed the hot plate test. Q.Y. performed the pupillary light reflex test. Z.Q., H.L., and X.L. performed the data analysis. Z.Q. and X.L. wrote the manuscript. Z.Q., Z.L., L.W., Y.C., and X.L. discussed the results and commented on the manuscript. Z.Q. and X.L. revised the manuscript. **Competing interests:** The authors declare that they have no competing interests. **Data and materials availability:** All data needed to evaluate the conclusions in the paper are present in the paper and/or the Supplementary Materials.

Submitted 13 April 2021
Accepted 1 September 2021
Published 22 October 2021
10.1126/sciadv.abi5811

Citation: Z. Qian, H. Li, H. Yang, Q. Yang, Z. Lu, L. Wang, Y. Chen, X. Li, Osteocalcin attenuates oligodendrocyte differentiation and myelination via GPR37 signaling in the mouse brain. *Sci. Adv.* **7**, eabi5811 (2021).